Improving the Performance of Wireless Systems via Selective Interference Nulling and Adaptive Medium Access Control Design

by
Sarfraz Ghani

Thesis Submitted to the Faculty of
Virginia Polytechnic Institute and State University
In partial fulfillment of the requirements of the degree of

MASTER OF SCIENCE
In
Electrical Engineering

Dr. Annamalai Annamalai
Dr. Jeffery H. Reed
Dr. Amir Zaghloul
June 26, 2006
Blacksburg, Virginia

Keywords: Wireless Communication, Smart Antenna, Adaptive Interference Nulling, Diversity Combining, Cross-layer Simulation

Improving the Performance of Wireless Systems via Selective Interference Nulling and Adaptive Medium Access Control Design

by

Sarfraz Ghani

Committee Chair: Dr. Annamalai Annamalai

Bradley Department of Electrical and Computer Engineering

ABSTRACT

Escalating demands for high performance wireless systems requires the confluence of smart communication methods, network protocols and ongoing advances in fabrication technologies, in order to bring smaller form factor mobile handsets to market. On par with these trends, this thesis focuses on two main areas, namely, Multiple Antenna Systems and Adaptive MAC Design to improve wireless system performance.

The first part of this research work presents a mathematical framework for characterizing the performance of cellular mobile radio systems equipped with smart antennas at the mobile handset to suppress a few dominant cochannel interferers (CCI) out of a total of L active independent but non-identically distributed Rayleigh faded CCI signals. Earlier works on this subject chose an unrealistic i.i.d assumption for the cochannel interferers. Since the CCI signals are of dissimilar signal strengths in practical operating environments, the premise of i.n.d fading statistics for the cochannel interferers is more realistic. In the subsequent section an analytical framework to investigate the benefits of a hybrid antenna array using selective interference nulling (SIN) and maximal ratio combining (MRC) in mobile radio environments is developed.

In the second part of this thesis, we explore the performance gains that can be achieved by exploiting the synergy resulting from the combination of the MAC and the physical layer of a wireless network. As in a traditional design, the physical layer is responsible for providing error protection for the transmission packets while the MAC layer allocates transmission bandwidth to the contending users. However, in the proposed scheme the MAC layer makes slot assignment decisions based on the channel state information (CSI) from the physical layer.

ACKNOWLEDGEMENT

First and foremost, I would like to thank Allah (s.w.t) for the innumerable bounties that he has bestowed upon me and my family and for giving me an opportunity to undergo higher education in a university of repute. I hope and wish that this education I have acquired would be beneficial to his creation in whatever form possible.

I would like to sincerely thank my primary advisor Dr. Annamalai Annamalai for his suggestions and advice on each part of this research, if not for his assistance and constructive criticisms this work would have been incomplete. I would also like to thank my committee members Dr. Jeffery Reed and Dr. Amir Zaghloul for their helpful suggestions.

I would like to acknowledge some of my fellow colleagues at MPRG for their generous help, Sudhanshu Gaur for his suggestions on Cross-layer simulation approaches for MANET. Venkat for sharing his expertise on the design methodology of an OFDM simulator and Ramanathan for being a very dear friend.

Last but not the least I owe every part of this work, my education and every step forward in life to my beloved mother. If not for her patience and utmost determination nothing of this would have ever been possible. I am also highly indebted to my sister, my aunts, my wife and my friends for their support.

TABLE OF CONTENTS

LIST OF FIGURES

LIST OF TABLES

Chapter 1

Introduction

Recent trends in the wireless industry point towards an urgent need to improve communication system performance with respect to capacity for high data rate 3G systems. To corroborate this urgency, current market leaders have already announced chip solutions integrating multiple antenna systems (receive diversity) at the mobile terminal. This in hand with advances in fabrication technologies has made possible the realization of small form factor mobile handsets incorporating multiple antennas. Such efforts have greatly improved forward link performance from the base-station to the mobile handset.

Given the indisputable advantages of deploying multiple antennas at the mobile terminal, it would be worthwhile to investigate in more detail the diversity gain and co-channel interference rejection capabilities offered by this technology. In regards to this, the first part of this research would delve into evaluating the performance of cellular mobile systems employing a selective interference cancellation (SIC) receiver. One of the major detriments towards improving capacity includes interference from co-channel cells and multipath fading. To mitigate these detrimental factors, cell sectorization, diversity mechanisms, and adaptive null steering techniques may be employed. However, cell sectorization reduces the trunking efficiency, while diversity methods are not very effective at low signal-to-interference ratio (SIR) levels. Moreover, the relative diversity improvement diminishes with increasing diversity order. The selective interference nulling scheme, in which the gain pattern of an antenna array is shaped by steering nulls in the direction of the dominant CCI signals without significantly attenuating the desired user signal, works best in an interference-limited scenario or in the presence of strong narrowband interferers. Earlier literature trying to evaluate the performance of a cellular system employing a SIC receiver worked on the assumption that the CCI signals are independent and identically distributed, this is a rather pessimistic approach. In practical operating environments the co-channel interferers are of unequal powers, hence the

assumption that the CCI signals are of independent and non-identical distribution fading statistics is more realistic. In this part of the research we present an analytical framework for characterizing the outage probability and average bit or symbol error rate in the presence of i.n.d Rayleigh faded CCI signals, the desired user signal could follow any arbitrary fading distribution.

Next, we would investigate a novel receiver technique exploiting the synergy between adaptive null steering and diversity combining. Given the exhaustive merits/demerits of these multiple antenna schemes and their quite opposite behavioral trends with respect to a given operating condition, such as strength of CCI signals, length of antenna array, faded distribution of desired user signal etc., it is in our best interest to exploit the best of both worlds. This chapter presents a hybrid AIN/MRC receiver and derives a generic expression for the moment generating function (m.g.f) of the SIR. The m.g.f obtained in this chapter is sufficiently general and can be used to study the probability of outage as well as average error rates for the hybrid scheme. The AIN alone and the MRC alone receivers are also treated as limiting cases.

The subsequent chapter demonstrates the design of various scheduling algorithms for wireless networks. Future, high speed data and multimedia applications would require that a particular quality of service (QoS) requirement be met. The use of scheduling strategies is an instinctive direction in the provision of guaranteed QoS parameters such as delay, packet loss rate and throughput [1]-[2]. Conventionally, scheduling is done at the multiple access control (MAC) layer where it judiciously arbitrates the requests of multiple users and assigns transmission bandwidth to the users. The arbitration, in this case is made independent of, the performance metrics of the underlying physical layer. These protocols work on the assumption that packet transmission by the physical layer is error-free. Unfortunately, this assumption does not hold for wireless networks where the physical layer performance is highly time variant. Motivated by this fact, this research work, explores the performance gains that can be achieved by exploiting the synergy resulting from the combination of the MAC and the physical layer of a wireless network with data services [3].

As in a traditional design, the physical layer is responsible for providing error protection for the transmission packets while the MAC layer allocates transmission bandwidth to the contending users. However, in the proposed scheme the MAC layer makes slot assignment decisions based on the channel state information (CSI) from the physical layer. Utilizing the CSI's of the contending users, the MAC layer allocates transmission bandwidth to the un-coordinated user with the best CSI, this mechanism makes use of the available bandwidth more effectively compared to approaches that independently model the MAC and the physical layer.

In this research work, OPNET is utilized for modeling the MAC layer, whereas, the entire physical layer simulator is written in MATLAB. OPNET is an event driven simulation tool. Since physical layer modeling is stochastic in nature, OPNET by itself does not provide a convenient platform for investigation. Thus as part of this work, techniques are explored for integrating traditional physical layer simulation tools, such as MATLAB, into OPNET to perform the necessary stochastic physical layer simulations.

1.1 Thesis outline

This manuscript is broadly classified into three main chapters the first two dealing with Multiple Antenna systems and the third with Adaptive MAC scheduling for wireless systems.

Chapter 2 is devoted to the performance evaluation of cellular mobile radio systems that implement a selective cochannel interference cancellation scheme. A comprehensive review of literature on CCI cancellation is first presented in Section 2.1. In Section 2.2, we derive the moment generating function (m.g.f), probability density function (p.d.f) and cumulative distribution function (c.d.f) of the sum of N "weakest" CCI signal powers as well as the p.d.f for the signal-to-interference ratio (SIR). Section 2.3 derives outage probability expressions for both the interference limited case as well as the scenario that takes into consideration the effect of receiver noise. In Section 2.4, we derive analytical

expressions for computing the average symbol error rate (ASER) of different digital modulation formats in a variety of fading environments. Section 2.5 presents selected numerical results illustrating the application of the theory developed in Sections 2.2 through 2.4 to cellular mobile radio design. Finally the main contributions and conclusions of this chapter are summarized in Section 2.5.

Chapter 3 develops an analytical framework for characterizing the performance of hybrid AIN/MRC (or EGC) diversity in a cellular mobile radio environment. An overview of AIN/MRC schemes and the merits/demerits of choosing between either of the two schemes in a given practical operating environment are discussed in Section 3.1. The subsequent section derives a generic closed form expression for the m.g.f of the SIR signal statistics that can be used for evaluating the performance of the hybrid scheme. Section 3.3 utilizes the m.g.f of the SIR obtained in Section 3.2 to come up with a simplistic probability of outage expression for the case where the desired user signal is Nakagami-m faded and the CCI signals follow i.i.d Rayleigh fading. Numerical plots for the outage probability of the hybrid receiver are also presented in this section. Section 3.4 presents probability of error expressions for both coherent and non-coherent receivers in terms of the m.g.f of the SIR, some numerical results showing the ABER curves for coherent/non-coherent receivers employing the hybrid AIN/MRC scheme are also given. Finally the chapter conclusion is presented in Section 3.5.

Chapter 4 examines a new holistic approach to MAC scheduling by exploiting the synergy resulting from the combination of the MAC and physical layer of a wireless network. A comprehensive literature review of different MAC scheduling approaches is presented in Section 4.1. Section 4.2 presents an overview of the system chosen, in order to demonstrate the approaches developed in this chapter including a detailed description of the physical layer. An overview of scheduler components and properties along with a description of the greedy algorithm simulated as part of this research is described in Section 4.3. Section 4.4 gives an overview of the methodologies and techniques used in developing the simulation of this system. Section 4.5 presents an overview of the steps

taken in implementing these simulation methodologies. Finally a summary of key results for cross-layer simulations using co-simulations is given in Section 4.6

Finally, Chapter 5 presents the thesis contributions and suggestions for future work.

Chapter 2

Performance Evaluation of Cellular Mobile Radio Systems with Selective Cochannel Interference Cancellation

2.1 Literature Review

In general, an adaptive antenna array with *D*-elements can effectively suppress (*D* - 1) dominant CCI signals [4]. As such, the performance capability of an antenna array system in the presence of a large number of CCI signals is restricted by the number of antenna elements. This is particularly important for mobile hand-held and portable terminals, since the ergonomic considerations such as size, complexity and cost will dictate the number of elements in an adaptive array receiver. This, combined with the fact that practical antenna arrays may have to operate in an environment with a large number of interferers, implies that a linear space-time adaptive processing will fail as the array's degree of freedom is exceeded. In this overloaded array situation, selective interference nulling of dominant CCI signals is attractive owing to its linear processing complexity compared to the existing complex overloaded array processing algorithms [5]-[6]. Moreover, portable radios that use smart antennas have system level benefits: interference suppression and spatial diversity permit the use of lower transmit power for a specified reliability. This decreases CCI level, increases the battery life of portable terminals, and reduces the probability that a hostile party will intercept the signals. Consequently, future generations of wireless communication systems are expected to take advantage of the significant performance and capacity gain promised by smart antennas at the mobile terminals.

In [7]-[8], the authors studied the outage performance of cellular mobile radio systems with selective interference cancellation (SIC) of dominant CCI signals in a Rayleigh fading environment. The analysis was extended in [9] to independent and identically distributed (i.i.d) Nakagami-m faded CCI signal amplitudes. It should be highlighted,

however, that the assumption of i.i.d fading statistics for the CCI signals in [7]-[9] portrays a pessimistic outage performance measure of practical operating environments. Since different CCI signals may take completely different propagation paths before arriving at the receiver, it is more reasonable to assume that the signals have dissimilar signal strengths. Despite this, neither analytical nor simulation results for independent but non-identically distributed (i.n.d) CCI signal statistics has been reported in the literature. In this chapter, we present an analytical framework for characterizing the outage probability and average bit or symbol error rate in the presence of i.n.d Rayleigh faded CCI signals. The closed form outage probability expressions (for the interference limited case as well as the case that treats receiver noise) are sufficiently general because they treat all common fading channel models for the desired user signal amplitude.

2.2 SIR Signal Statistics

Consider a cellular mobile radio environment where the desired user cell is surrounded by L co-channel cells in the first and second tiers. Let us further assume that the desired user signal amplitude is subject to slow varying flat Rayleigh, Rician (with Rician factor K_o), Nakagami-m (with fading parameter m_o) or Nakagami-q (with fading parameter q_o) type of fading with the average fading power of $\overline{p}_o$, whereas the L active interfering signals are assumed to be independent and to be subject to slowly varying flat Rayleigh fading. Moreover, the instantaneous signal powers p_k $(1 \le k \le L)$ are modeled as i.n.d exponential random variates with p.d.f $f_k(.)$ and c.d.f $F_k(.)$ as shown below:

$$f_k(x) = \frac{1}{\overline{p}_k} e^{-x/\overline{p}_k}, \quad 0 \le x < \infty, \; k \in \{1, 2, ..., L\} \tag{1}$$

$$F_k(x) = 1 - e^{-x/\overline{p}_k}, \; 0 \le x < \infty, \; k \in \{1, 2, ..., L\} \tag{2}$$

where $\overline{p}_k$ denotes the average power of the k-th CCI signal.

Suppose a mobile terminal in the desired user cell is equipped with an antenna array consisting of D elements, we assume that the smart antenna can effectively suppress (D - 1) strongest CCI signals. Thus, the performance of the mobile radio system will be dictated by the $N = L - D + 1$ uncancelled (residual) CCI signals, viz.,

$$I = \sum_{i=1}^{N} p_{i:L} \tag{3}$$

where $p_{i:L}$ denotes the *i*-th order statistic (obtained by ranking the CCI instantaneous signal powers in ascending orders of magnitude as $0 \le p_{1:L} \le p_{2:L} \le ... \le p_{L:L} \le \infty$). It should be highlighted, that, in contrast to previous studies [7]-[9], in this chapter we move away from the i.i.d restriction for the CCI signal statistics, while the desired user signal amplitude may assume any common fading distribution. In particular, we generalize the analysis and results presented in [8] by taking into account of the power imbalance among the CCI signals. This assumption is more realistic and a good representative of the practical mobile radio operating environments.

Suppose we denote the instantaneous received power for the desired user signal by p_o, then the SIR is defined as $\gamma = p_o / I$. The statistics of SIR are important for quantifying the outage probability as well as the average symbol or bit error rate performance of the cellular mobile radio system equipped with a smart antenna. In order to obtain explicit formulas for the p.d.f of the SIR, we first require the statistics of *I*. In the following subsections, we derive the m.g.f, p.d.f and c.d.f of *I* and subsequently use these expressions for deriving a closed form formula for the p.d.f of SIR, which holds for a variety of fading distributions for the desired user signal amplitude.

2.2.1 Ordered CCI Signal Statistics

The joint p.d.f of the order statistics $p_{1:L} \le p_{2:L} \le ... \le p_{L:L}$ at $x_1, x_2, ..., x_L$ is given by [10]

$$f_{p_{1:L}, p_{2:L}, ..., p_{L:L}}(x_1, x_2, ..., x_L) = per\left(\begin{bmatrix} f_1(x_1) f_2(x_1) ... f_L(x_1) \\ f_1(x_2) f_2(x_2) ... f_L(x_2) \\ . \\ f_1(x_L) f_2(x_L) ... f_L(x_L) \end{bmatrix} \right) = \sum_{\sigma \in S_L} \prod_{i=1}^{L} f_{\sigma(i)}(x_i) \tag{4}$$

where $0 \le x_1 \le x_2 \le ... \le x_L < \infty$, $per([A])$ denotes the permanent of a square matrix *A*, S_L is a symmetric group of degree L which permutes integers $1, 2, ..., L$ and $\sigma = \{\sigma(1), ..., \sigma(L)\}$ in the sum of (4) runs over all *L!* members of S_L. The process of

constructing all members of S_L is recursive and most common mathematical software packages have explicit commands for this purpose. For instance S_L can be constructed using perms $([1,2,...,L])$ in MATLAB.

Utilizing the joint p.d.f of the order statistics obtained in (4), we can readily evaluate the m.g.f of I as

$$\phi_I(s) = E\left[\exp(-sI)\right] = \sum_{\sigma \in S_L} \int_{0<x_1<x_2..<x_L<\infty} ..\int e^{-s\sum_{i=1}^{N} x_i} \prod_{i=1}^{L} f_{\sigma(i)}(x_i) dx_L ... dx_2 dx_1 \,,\ s>0 \qquad (5)$$

where $E[.]$ denotes the ensemble average of its argument.

Substituting (1) into (5), and after standard mathematical manipulations (i.e., evaluating the nested integral recursively) we obtain

$$\phi_I(s) = \sum_{\sigma \in S_L} \frac{\prod_{k=1}^{L} \left(1 \Big/ \overline{p}_k \right)}{\underbrace{\theta_1 \theta_2 ... \theta_{L-N}}_{(L-N)terms} \underbrace{(s+\theta_{L-N+1})(2s+\theta_{L-N+2})...(Ns+\theta_L)}_{(N)terms}}$$

$$= \sum_{\sigma \in S_L} \frac{\prod_{k=1}^{L} \frac{1}{\overline{p}_k}}{\prod_{i=1}^{L-N} \theta_i} \prod_{k=1}^{N} \frac{1}{(ks+\theta_{L-N+k})} \qquad (6)$$

where $\theta_k = \sum_{i=0}^{k-1} \frac{1}{\overline{p}_{\sigma(L-i)}}$ for $k = 1,2,...,L$.

It is clear that for the case of i.i.d fading, $\overline{p}_1 = \overline{p}_2 = ... = \overline{p}_L = \overline{p}$, $\theta_k = \frac{k}{\overline{p}}$ and there will be $L!$ equal terms in the summation of (6). Therefore (6) reduces into

$$\phi_I(s) = \prod_{k=1}^{N} \left[1 + \frac{ks\overline{p}}{L-N+k} \right]^{-1} \qquad (7)$$

Eq. (7) is in agreement with [9, Eq. (B.6)] and [8, Eq. (66)].

Now let us turn our attention back to the i.n.d case. Expanding (6) using partial fractions, we obtain

$$\phi_I(s) = \sum_{\sigma \in S_L} \sum_{k=1}^{N} \frac{k\eta_k}{(ks+\theta_{L-N+k})} \qquad (8)$$

where $\eta_k = \dfrac{\prod_{k=1}^{L} \dfrac{1}{\overline{p}_k}}{\left[\prod_{k=1}^{L-N} \theta_k\right] N!} \prod_{\substack{i=1 \\ i \neq k}}^{N} \dfrac{ki}{k\theta_{L-N+i} - i\theta_{L-N+k}}$

Now taking the inverse Laplace transform of (8), we immediately get a closed form expression for the p.d.f of *I*, viz.,

$$f_I(x) = \sum_{\sigma \in S_L} \sum_{k=1}^{N} \eta_k e^{-x\theta_{L-N+k}/k}, \quad 0 \leq x < \infty \tag{9}$$

The corresponding c.d.f is given by

$$F_I(x) = 1 - \sum_{\sigma \in S_L} \sum_{k=1}^{N} \eta_k \frac{k e^{-x\theta_{L-N+k}/k}}{\theta_{L-N+k}}, \quad 0 \leq x < \infty \tag{10}$$

Before concluding this subsection, we would like to point out that the number of summands in (6) or (8) grows exponentially with increasing *L*. This clearly motivates the derivation of alternative closed form expressions for $\phi_I(s)$ which are numerically efficient for large *L*. Two such formulas are provided in Appendix A. These expressions may be used in conjunction with [9, Eqs. (2) and (13)] for outage probability analysis. In the following subsection, we will utilize (9) to derive a closed form expression for the p.d.f of SIR.

2.2.2 SIR Statistics

In this subsection, we derive a unified expression for the p.d.f of the SIR assuming that the CCI signal amplitudes are subject to i.n.d Rayleigh fading but the desired user signal amplitude follows either Rayleigh, Rician, Nakagami-m or Nakagami-q distribution. This expression in turn, may be used for outage analysis (discussed in detail in Section III) or for ASER analysis (see Section IV).

If the p.d.f of p_o (i.e., $f_o(.)$) and $f_I(.)$ are known, then the p.d.f of SIR $\gamma = p_o / I$ may be evaluated as

$$f_\gamma(\gamma) = \int_0^\infty x f_o(\gamma x) f_I(x) dx \tag{11}$$

Substituting (9) into (11) and using variable substitution $y = \gamma x$, we get a closed form formula for the p.d.f of γ, viz.,

$$f_\gamma(\gamma) = \frac{-1}{\gamma^2} \sum_{\sigma \in S_L} \sum_{k=1}^{N} \eta_k \phi_o^{(1)} \left(\frac{\theta_{L-N+k}}{k\gamma} \right) \tag{12}$$

where $\phi_o^{(1)}(a) = \frac{d}{ds} \phi_o(s)\big|_{s=a}$ denotes the first order derivative of the m.g.f of p_o with respect to s and then evaluating the resulting expression at $s = a$. It should be emphasized that the above p.d.f can be evaluated in closed form for all common fading models for the desired user signal owing to the availability of closed form formulas for the first order derivative of the m.g.f of the desired user signal power (see Table II in [11]). It is also possible to obtain a generic expression for the c.d.f of γ similar to (12). To do so, we exploit identity (B.4) to get (13) from (12) by observation:

$$F_\gamma(x) = \int_0^x f_\gamma(y)dy = \sum_{\sigma \in S_L} \sum_{k=1}^{N} \frac{k\eta_k}{\theta_{L-N+k}} \phi_o \left(\frac{\theta_{L-N+k}}{kx} \right) \tag{13}$$

2.3 Outage Analysis

In this section, we derive closed form expressions for computing the probability of outage in picocellular, microcellular and macrocellular environments in terms of only the marginal m.g.f of p_o, which is defined as $G_o(s,x) = \int_x^\infty \exp(-sp_o/q) f_o(p_o) dp_o$. Clearly, $\phi_o\left(s/q\right) = G_o(s,0)$ and the c.d.f of p_o is related to the marginal m.g.f as $F_o(x) = 1 - G_o(0,x)$.

2.3.1 Interference Limited Environment

In an interference-limited (picocellular and microcellular) environment, satisfactory reception is assumed to be achieved as long as the short-term SIR exceeds the CCI power

protection ratio q (neglecting the receiver background noise). Hence the outage event is given by

$$P_{out}(N,L) = F_{\gamma}(q) = \sum_{\sigma \in S_L} \sum_{k=1}^{N} \frac{k\eta_k}{\theta_{L-N+k}} \phi_o\left(\frac{\theta_{L-N+k}}{kq}\right) \tag{14}$$

where $\phi_o(.)$ is the m.g.f of the desired user signal power (available in closed form for a myriad of fading environments and they are summarized in Table II of [11]).

In practice, thermal noise (receiver noise) always exists which may be of concern in macrocellular environments. In the literature, this effect is considered either by imposing an additional minimum desired signal power requirement for satisfactory reception [12] or by treating receiver noise as CCI [13]. These cases are also treated in the following subsections.

2.3.2 Minimum Signal Power Requirement

The probability of outage with a minimum desired signal power constraint can be computed by formulating the outage problem in the framework of hypothesis testing. The outage event in this case is given by

$$\begin{aligned} P_{out}(N,L) &= F_o(\Lambda) + \int_{\Lambda}^{\infty} f_o(p_o) F_I^{(c)}(p_o/q) dp_o \\ &= F_o(\Lambda) + \sum_{\sigma \in S_L} \sum_{k=1}^{N} \frac{k\eta_k}{\theta_{L-N+k}} G_o\left(\frac{\theta_{L-N+k}}{k}, \Lambda\right) \end{aligned} \tag{15}$$

where $F_I^{(c)}(x) = 1 - F_I(x)$ denotes the complementary c.d.f of I and Λ corresponds to the minimum desired signal power level for satisfactory reception (due to receiver noise). Note that $G_o(s,x)$ is convergent and a closed form expression for this quantity is known if the desired signal amplitude is subject to Rayleigh, Rician, Nakagami-m or Nakagami-q fading (see Table I of [10]). Obviously by setting $\Lambda = 0$, (15) reduces to (14) as expected (i.e., interference limited case).

2.3.3 Treating Receiver Noise as CCI

To incorporate the effect of receiver noise as a CCI signal, the outage event in the interference limited case must be redefined as $\Pr\{p_o < qI + \Lambda\}$ where Λ is a product of the total noise power and the noise power protection margin. It is apparent that specifying a receiver noise threshold will cause a floor on the outage probability regardless of whether CCI is present or not because the deep fades will result in signal power level below the specified minimum level. In fact, this floor dictates the outage performance in a noise-limited case. It is not difficult to show that the probability of outage in this case is given by

$$P_{out}(N,L) = F_o(\Lambda) + \int_{\Lambda}^{\infty} f_o(p_o) F_I^{(c)}((p_o - \Lambda)/q) dp_o$$

$$= F_o(\Lambda) + \sum_{\sigma \in S_L} \sum_{k=1}^{N} \frac{k\eta_k}{\theta_{L-N+k}} \exp\left(\frac{\Lambda \theta_{L-N+k}}{kq}\right) G_o\left(\frac{\theta_{L-N+k}}{k}, \Lambda\right) \qquad (16)$$

2.4 ASER Analysis

ASER is another useful performance measure of digital modulation schemes in cellular mobile radio systems. In general, the ASER can be calculated by averaging the conditional error probability (i.e., performance in additive white Gaussian noise channel) over the p.d.f of SIR, viz.,

$$\overline{P}_s = \int_0^{\infty} P_s(\gamma) f_\gamma(\gamma) d\gamma \qquad (17)$$

where $P_s(.)$ denotes the conditional error probability. It is apparent that if $P_s(.)$ is available in closed form, then the ASER may be computed using (17) and (12) (i.e., a single integral formula) while the desired user signal amplitude is subject to Rayleigh, Rician, Nakagami-m or Nakagami-q distribution. Similarly if $\frac{d}{d\gamma} P_s(\gamma)$ is available in closed form, then the ASER may also be evaluated via a single integral expression as $\overline{P}_s = -\int_0^{\infty} F_\gamma(\gamma) \left[\frac{d}{d\gamma} P_s(\gamma)\right] d\gamma$ (obtained from (17) using integration by parts) and using (13).

Alternatively, using the m.g.f based performance evaluation technique, we may compute the ASER for a broad range of coherent, differentially coherent and non-coherent modulation schemes in terms of only $\phi_\gamma(.)$. However, it appears that a closed form solution for $\phi_\gamma(.)$ is only available for the special case of Nakagami-m faded desired user signal amplitude (includes Rayleigh fading when m_o = 1). In this case, (12) may be simplified as

$$f_\gamma(\gamma) = \frac{\Gamma(1+m_o)}{\Gamma(m_o)}\left(\frac{m_o}{\overline{p}_o}\right)^{m_o} \gamma^{m_o-1} \sum_{\sigma\in S_L}\sum_{k=1}^{N} \eta_k \left(\frac{\theta_{L-N+k}}{k} + \frac{m_o\gamma}{\overline{p}_o}\right)^{-1-m_o} \tag{18}$$

Next, using (18) and [14, Eq. (13.2.5)], we obtain the m.g.f of SIR in closed form:

$$\phi_\gamma(s) = \int_0^\infty f_\gamma(\gamma)\exp(-s\gamma)d\gamma = \Gamma(1+m_o)\sum_{\sigma\in S_L}\sum_{k=1}^{N}\frac{k\eta_k}{\theta_{L-N+k}}\psi\left(m_o, 0, \frac{s\overline{p}_o\theta_{L-N+k}}{km_o}\right) \tag{19}$$

where $\psi(.;.;.)$ denotes the confluent hypergeometric function of the second kind. Note that $\psi(.;.;.)$ can be readily evaluated in terms of the generalized hypergeometric function using the identity [14, Eq. (13.1.10)], viz.,

$$\psi(a;b;z) = z^{-a}\,{}_2F_0(a, 1+a-b;;-1/z) \tag{20}$$

For example, the ASER of M-ary phase shift keying (M-PSK) may be computed (via a single integral formula) as

$$\overline{P}_s = \frac{1}{\pi}\int_0^{\pi-\pi/M_c} \phi_\gamma\left(\frac{\sin^2(\pi/M_c)}{\sin^2\theta}\right)d\theta \tag{21}$$

where M_c denotes the alphabet size. It is straightforward to extend this result to other digital modulation schemes. They are omitted here for brevity.

2.5 Numerical Results and Remarks

Selected numerical results for the outage probability and the ASER with SIC receiver is presented next. To study the performance of selective interference nulling of dominant interferers with i.n.d fading statistics, it is plausible to introduce an exponentially decaying power model for modeling the power imbalances across the *L* CCI signals

because a single parameter $\delta > 0$ can capture this effect. Suppose the average power of the *k*-th CCI signal is $\overline{p}_k = Ce^{-k\delta}$, we need to choose *C* such that it satisfies the constraint $\sum_{k=1}^{L} \overline{p}_k = \overline{I}_T$. Solving for *C* yields,

$$\overline{p}_k = \frac{(1-e^{-\delta})e^{-k\delta}}{e^{-\delta} - e^{-(L+1)\delta}} \overline{I}_T \qquad (22)$$

where $\overline{I}_T$ denotes the sum of all the average CCI signal powers. Notice also that the receiver performance for the i.i.d case can be evaluated using (22) as a limiting case when $\delta \to 0$. For numerical computation purposes, it is appropriate to choose $\delta = 10^{-4}$ as a representative of the i.i.d case. For convenience, let us also define the normalized average SIR as $L\overline{p}_o / \overline{I}_T$ (which corresponds to the ratio between the average power of the desired user signal and the average power of a CCI signal).

2.5.1 Outage Probability with a Fixed Number of Interferers

Figure 2-1 illustrates the probability of outage curves for all three cases discussed in Section III, with and without taking into consideration the effect of power imbalances across the CCI signals. As expected, there is a noise floor on the outage probability at higher SIR/q in the presence of receiver noise. This is owing to the fact that the system performance at lower SIR/q is interference limited whereas the performance at higher SIR/q is noise limited. Also, observe that the outage performance curves obtained by treating receiver noise as CCI tends to be slightly pessimistic compared to the minimum signal power constraint assumption and the discrepancy is larger at the knee of the curves. Figure 2-1 also reveals that SIC receiver is more effective when there are large power imbalances across the *L* active CCI signals. Comparison between $\delta = 1$ and $\delta = 10^{-4}$ (i.i.d case) curves indicates that there are approximately an order of magnitude improvement (dB scale) in outage probability metric over the i.i.d CCI signals case with a 4-element antenna array due to the power imbalance across the CCI signals. It is also evident from the figure that the outage floor is reached at relatively lower values of normalized average SIR/q as δ increases for a fixed *N* as one may anticipate.

Figure 2-2 depicts the outage probability in a Rician/Rayleigh fading channel model with and without SIC. This plot clearly highlights the outage performance of two different interference cancellation strategies (i.e., SIC and random cancellation of CCI signals without ranking). As an example, let us consider the case of a two-element antenna array in the presence of six i.i.d CCI signals. If the antenna array randomly suppresses one of the CCI signals, the outage performance of the system will be equivalent to that of a mobile radio system with five CCI signals with no interference suppression. The other strategy is to have the antenna array to rank the CCI signals and subsequently suppress the CCI signal having the largest instantaneous power. In the latter strategy, the performance will be dictated by the remaining ($L - D + 1$) uncancelled interferers. Numerical results reveal that the interference rejection of the strongest CCI signals ($L = 6$, $N = 5$) scheme tends to outperform the case with random cancellation of the CCI signal ($L = 5$, $N = 5$). Moreover, if the CCI signals are now assumed to be i.n.d (by introducing power imbalances across the CCI signals), significant reduction in the normalized average SIR/q requirement can be realized for a specified outage rate. The relative improvement increases with a larger power imbalance.

2.5.2 Outage Probability with Random Number of Interferers

In practice, not all of the L CCI signals will be active at the same time. This is particularly true if the traffic loads in the cochannel cells are not heavy or when a discontinuous transmission scheme is implemented to improve the spatial efficiency. If M denotes the number of active CCI signals at a given time, then the outage event may be computed as [15]

$$P_{out} = \sum_{M=D}^{L} \binom{L}{M} B^{\frac{M}{N_c}} \left(1 - B^{\frac{1}{N_c}}\right)^{L-M} P_{out}(M - D + 1, M) \qquad (23)$$

where D denotes the number of elements in the antenna array, B is the blocking probability and N_c corresponds to the number of distinct frequency voice channels. Figure 2-3 illustrates the outage probability versus normalized average SIR/q curves in a Nakagami-m/Rayleigh fading channel model for two different blocking probabilities. For

a fixed *D*, it is observed that the discrepancy between the curves corresponding to $B = 0.5$ and $B = 0.02$ diminishes as δ gets larger. Although a higher value of *B* corresponds to a larger number of channels being active, a larger δ also indicates that there are only a few strong CCI signals for a fixed normalized average SIR/q. Therefore, as δ gets larger, a larger *B* does not significantly degrade system performance.

2.5.3 Reuse Distance and Spectral Utilization Efficiency

In a cellular system with a uniform deployment of hexagonal cells, the spectral efficiency is given by [16]

$$\eta = \frac{G_c}{\sqrt{3} N_c W_c R^2 R_f^2} \; Erlang / MHz / km^2 \tag{24}$$

where G_c denotes the offered traffic per cell, N_c corresponds to the number of voice channels per cell, W_c is the bandwidth per channel (MHz), R is the distance from the center to the corner of a cell (i.e., cell radius) and R_f is the co-channel reuse factor. Considering a two slope model, [16] has shown that the normalized average SIR is related to cochannel reuse factor as

$$\frac{L\overline{p}_o}{\overline{I}_T} = (R_f - 1)^a \left(\frac{g/R + R_f - 1}{g/R + 1} \right)^b \tag{25}$$

where *a* and *b* are the path loss exponents and *g* denotes the breakpoint distance.

Using (24) and (25) in conjunction with (14), (15) or (16), the dependence of outage probability on the cochannel reuse factor as well as spectral efficiency can be studied. For example, Fig. 4 shows the outage probability curves as a function of cochannel reuse factor in a Nakagami-m/Rayleigh fading channel model with $\delta = 1$. Observe that, for a specified target outage, the cochannel reuse factor can be reduced dramatically by increasing the number of antenna array elements (i.e., by suppressing more dominant CCI signals). This indirectly translates into a higher spectral efficiency as evident from (24). In fact, the cochannel reuse factor R_f is directly related to the cluster size $C \in \{1, 3, 4, 7, 12, \ldots\}$ (Note: $C = i^2 + j^2 + ij$, i and j are non-negative integers) as $C = R_f^2 / 3$ for hexagonal cells deployment. A smaller *C* corresponds to a higher spectral efficiency but this is achieved at the expense of increased cochannel interference. However, since a SIC

receiver can effectively suppress dominant interferers, we can achieve a specified outage at a smaller R_f, or correspondingly achieve a higher spectral efficiency. For example, if target outage is specified to be 0.01, the cluster size can reduced from 12 to 7 by increasing the number of antenna element at the receiver from 1 to 3. (R_f = 5.3 for D = 1 and R_f = 3.7 for D = 3 are interpolated from Figure 2-4). This in turn highlights the benefits of smart antenna deployment in cellular radio systems.

In Figure 2-5, the outage probability is plotted as a function of spectral efficiency in a Rician/Rayleigh channel model. It is apparent that at a target outage of 0.05 and $\delta = 0$, we can realize approximately 166% improvement in the spectral utilization efficiency using 4-element antenna array compared to the omni-direction antenna (D = 1) case. If there are power imbalances among the CCI signals, the improvement will be even greater. For instance, the spectral efficiency improvement is approximately 200% when $\delta = 0.5$ at the same target outage and D = 4.

2.5.4 Average Error Rates

Figure 2-6 illustrates the average bit error rate versus the normalized average SIR curves for DPSK modulation in a Nakagami-m/Rayleigh fading channel model. The figure clearly highlights the benefits of employing a SIC receiver particularly when there are only a few dominant and many weak CCI signals. Other observations drawn from Figure 2-2 may also be inferred from this figure.

Figure 2-7 depicts the ASER performance of 8-PSK with SIC receiver versus normalized average SIR for a Nakagami-m faded desired user signal (m_o = 1.5) and $\delta = 1$. It is apparent that about 5dB gain can be realized by canceling only the strongest CCI signal (D = 2) over the normalized average SIR requirement for satisfying a prescribed grade-of-service (GoS) with no CCI cancellation (D = 1) at a target ASER of 0.01. Observe that the relative normalized average SIR improvement gets larger as additional CCI signals are cancelled. For instance, the relative gains are 9.8dB and 14.6dB while D = 3 and D = 4 respectively, at the same target ASER. This clearly highlights the merits of using a SIC receiver with higher number of antenna elements so as to achieve a significantly better

performance if size, cost and complexity considerations are not major factors in the design.

2.6 Chapter Conclusion

This chapter outlines an analytical framework for studying the outage and ASER performance of a cellular mobile radio system in overloaded array environments. Generic closed form expressions for the p.d.f and c.d.f of SIR at the output of a *D*-element antenna array is derived. Selected design examples are provided to show the benefits of a SIC scheme (in terms of communication link quality improvement without compromising the spectrum utilization efficiency, extended range and/or battery life) for cellular mobile radio communications. Our numerical results reveal that the power imbalance among the CCI signals play a significant role in the performance assessment of cellular radio system equipped with a SIC receiver. In particular we show that performance prediction with the i.i.d assumption for the CCI signal statistic when a SIC receiver is employed is very pessimistic. As such, any performance analysis must be revamped to account for the effects of unequal mean received powers among the CCI signals. This observation differs from the general trend that the outage and ASER performance in an interference limited environment is relatively insensitive to fading statistics of the CCI signals, and highlights the need to model both the desired user signal and CCI signals accurately for reliable performance prediction.

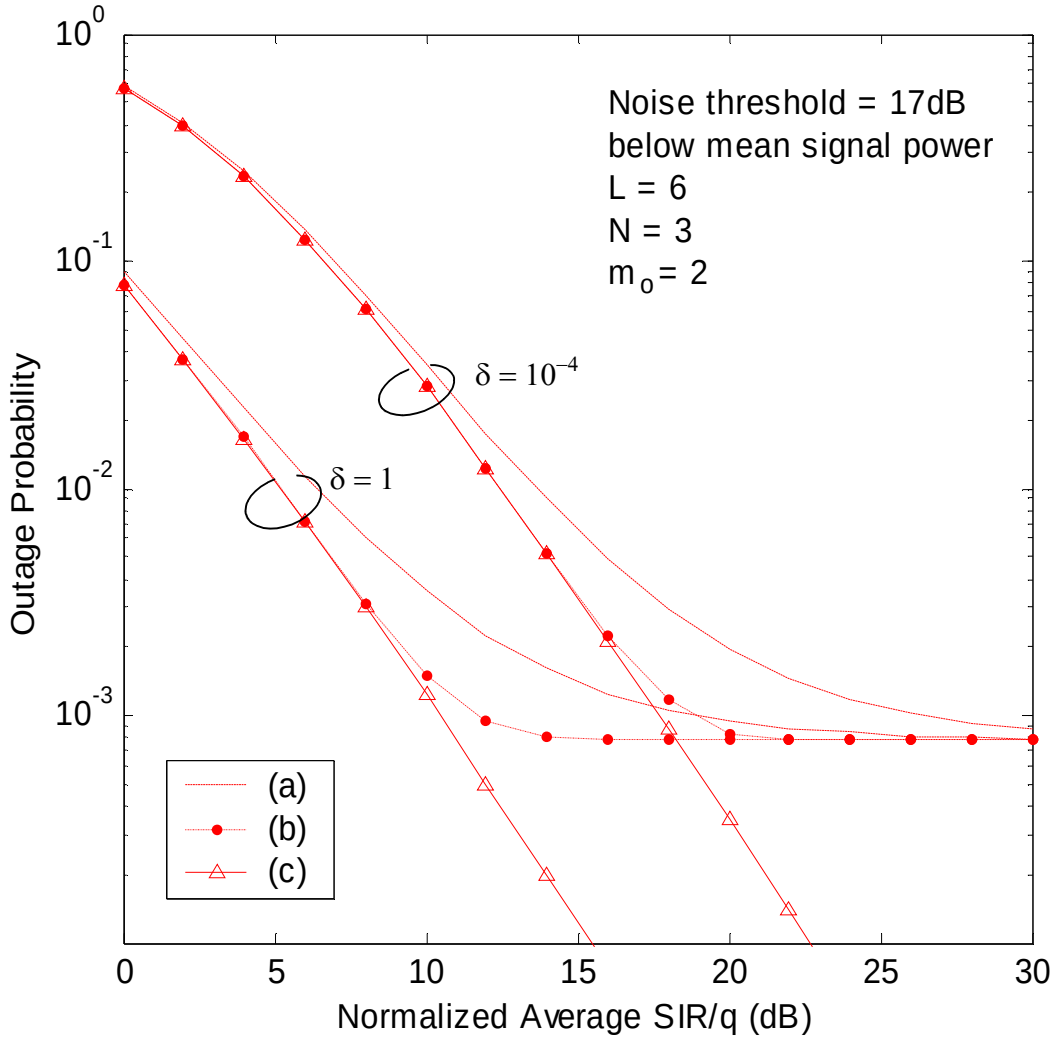

Figure 2-1 Outage probability versus normalized average SIR/q in a Nakagami-m/Rayleigh fading channel model: (a) treating receiver noise as CCI; (b) receiver noise is considered by imposing a minimum signal power constraint; (c) interference limited case

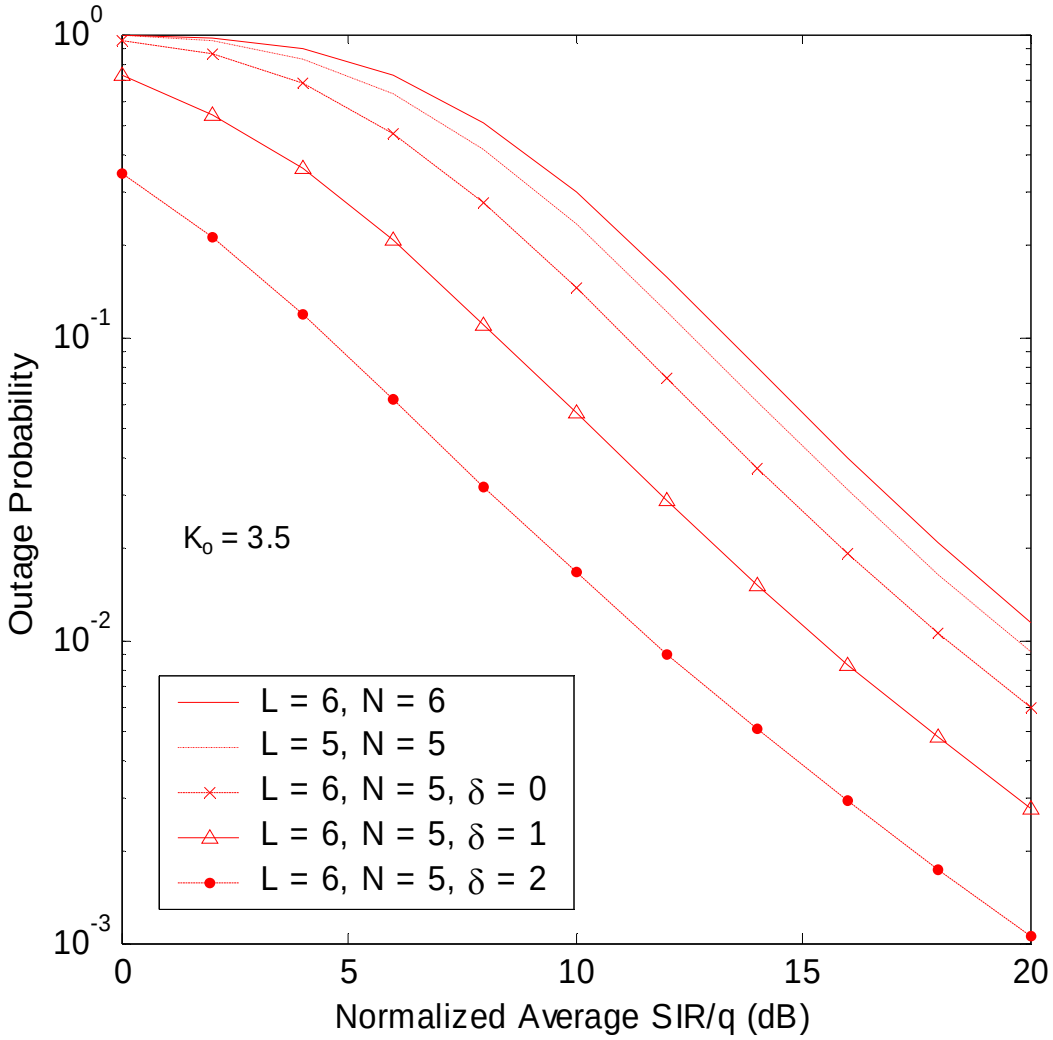

Figure 2-2 Outage probability versus normalized average SIR/*q* for an interference limited case in a Rician/Rayleigh fading channel model

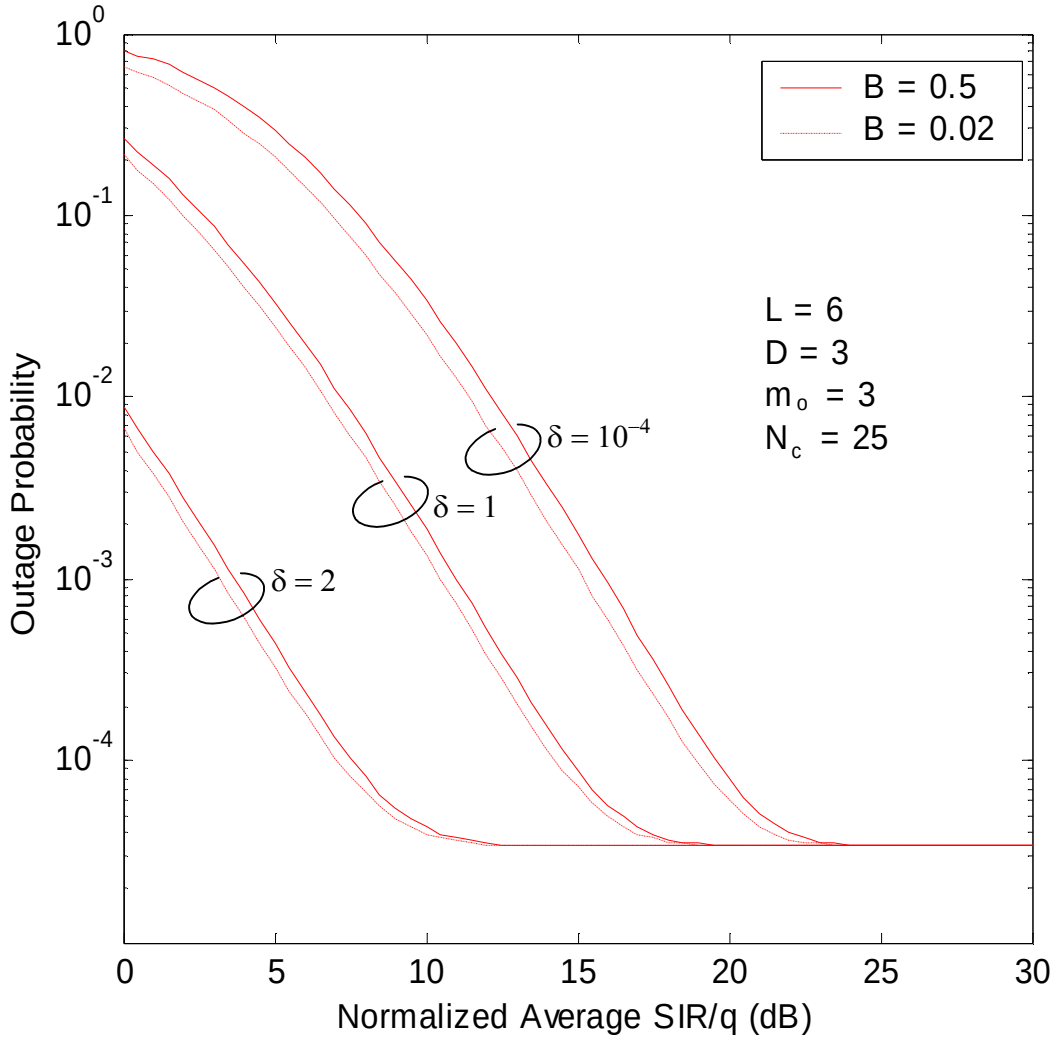

Figure 2-3 Outage probability versus normalized average SIR/q for different blocking probabilities $B \in \{0.5, 0.02\}$ by imposing a minimum signal power constraint in a Nakagami-m/Rayleigh fading channel model

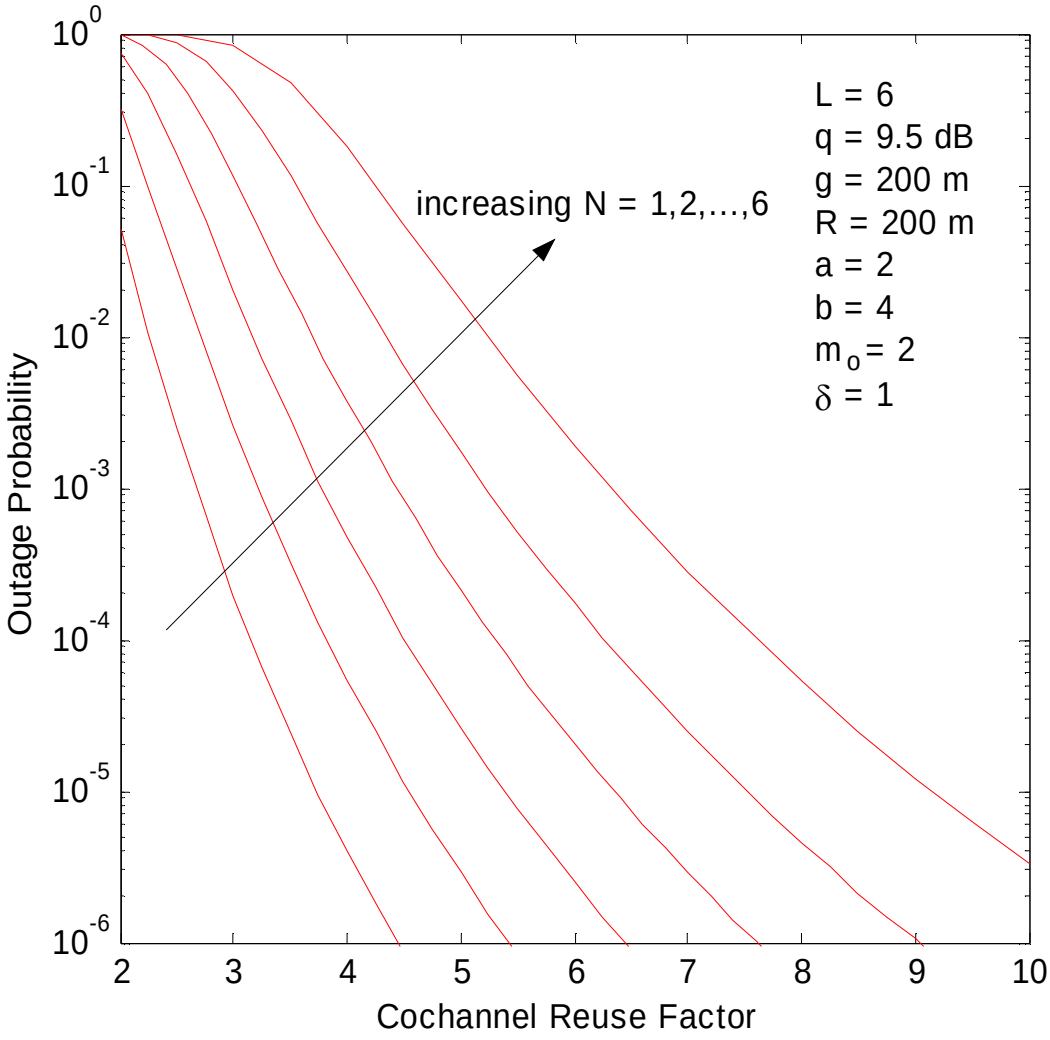

Figure 2-4 Outage probability as a function of cochannel reuse factor in a Nakagami-m/Rayleigh fading channel model

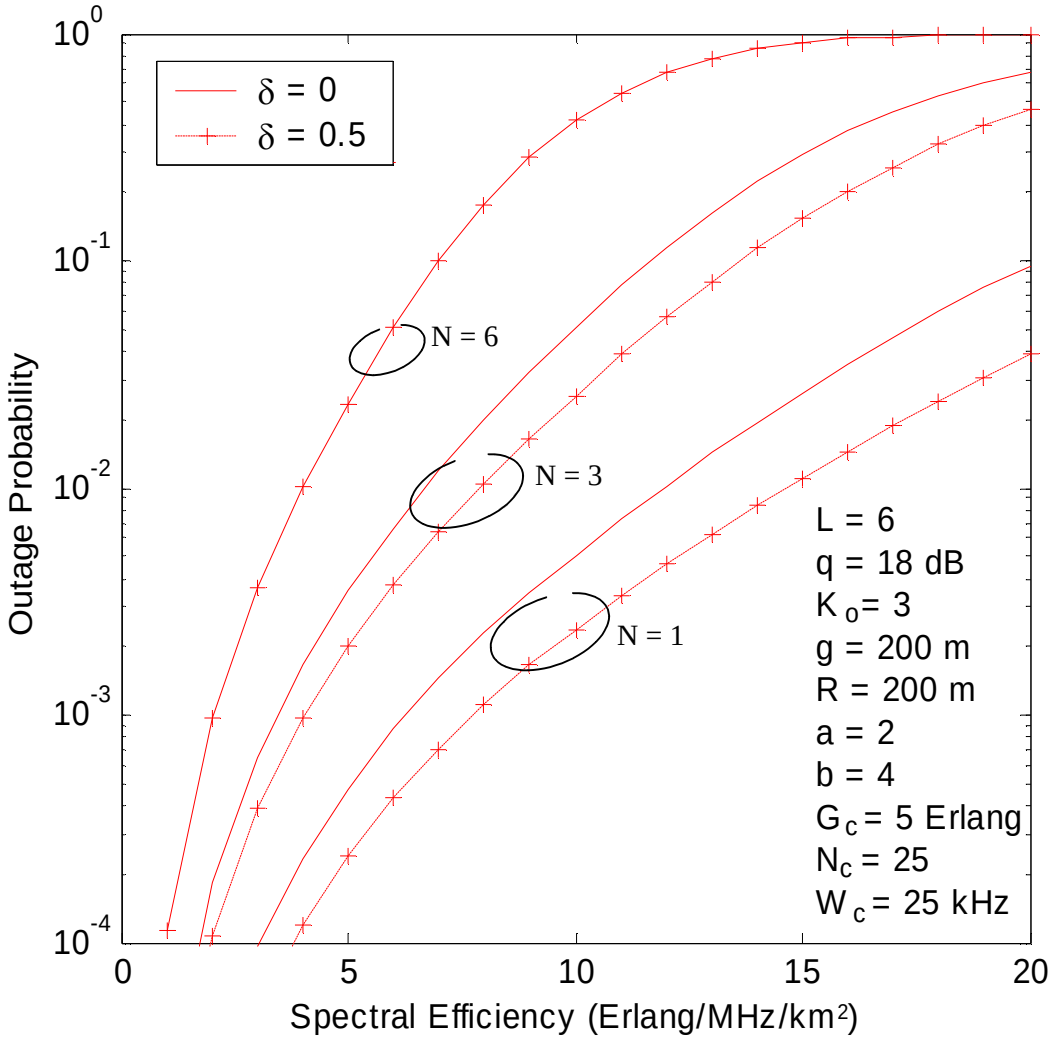

Figure 2-5 Outage probability versus spectral efficiency in a Rician/Rayleigh fading channel model

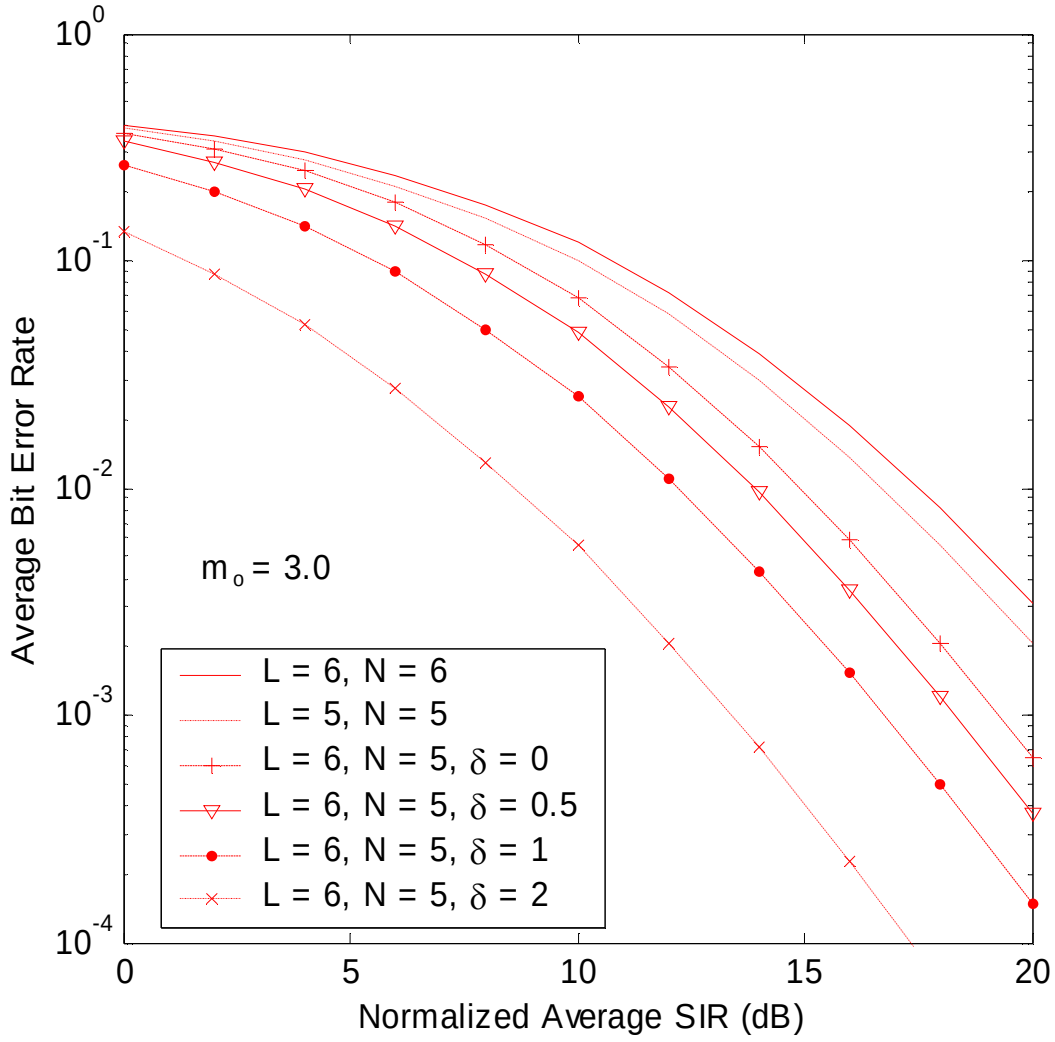

Figure 2-6 Average bit error rate versus normalized average SIR for DPSK modulation in a Nakagami-m/Rayleigh fading channel model

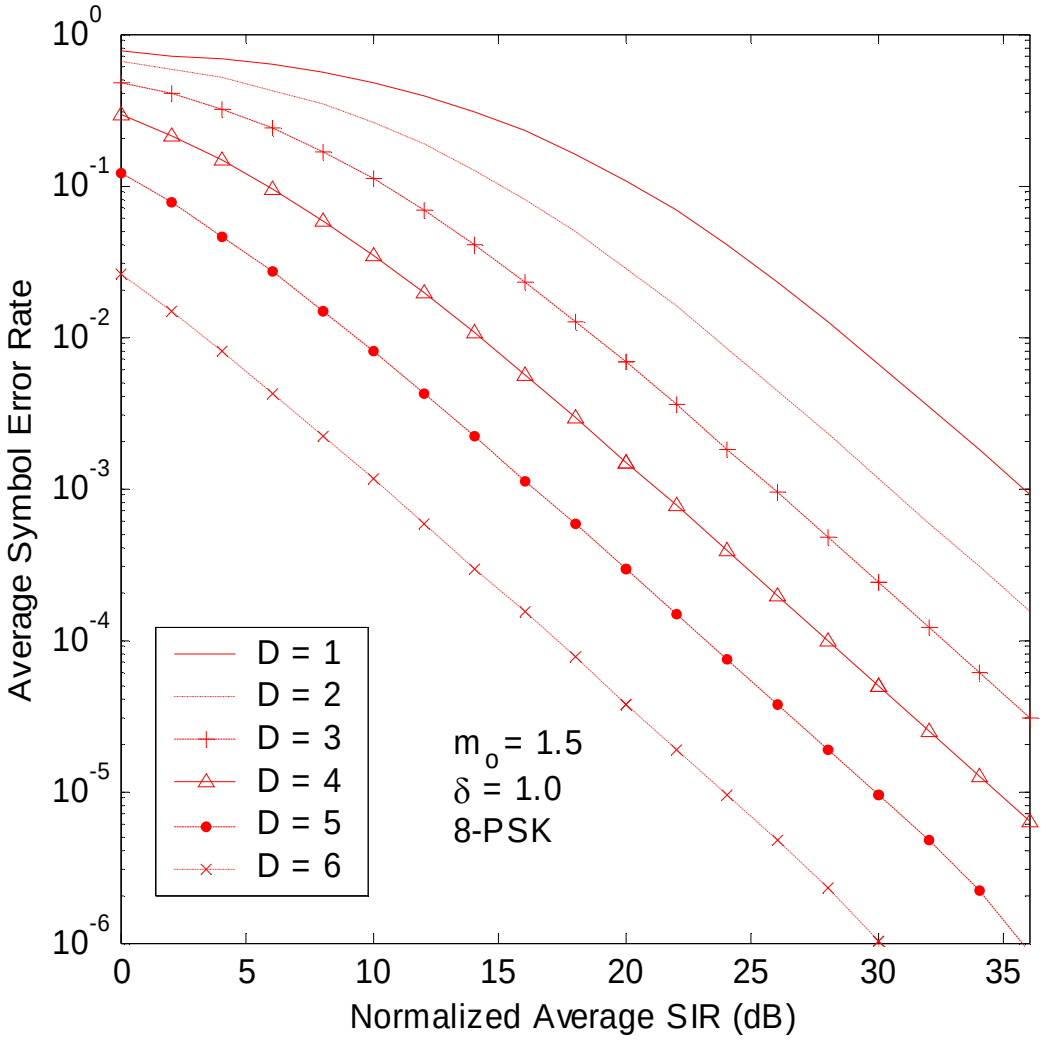

Figure 2-7 Average symbol error rate versus normalized average SIR for 8-PSK modulation in a Nakagami-m/Rayleigh fading channel model

Appendix A

Two attractive features of (8) is that it is very concise and it can be easily implemented in MATLAB within a few command lines. However, note that its computational complexity increases exponentially with L. For instance, the number of summation terms increases from 4! = 24 for L = 4 to 9! = 362880 with L = 9. This clearly motivates the derivation of a much more computationally efficient closed form expression for $\phi_I(s)$. In this appendix, we present two additional closed form expressions for $\phi_I(s)$ that require far fewer summation terms compared to (8).

To do so let us first rewrite (5) as

$$\phi_I(s) = \sum_{\sigma\in S_L} \int_0^{\infty} \frac{1}{\overline{p}_{\sigma(L)}} e^{-x_L/\overline{p}_{\sigma(L)}} \int_0^{x_L} \frac{1}{\overline{p}_{\sigma(L-1)}} e^{-x_{L-1}/\overline{p}_{\sigma(L-1)}} \ldots \int_0^{x_{N+2}} \frac{1}{\overline{p}_{\sigma(N+1)}} e^{-x_{N+1}/\overline{p}_{\sigma(N+1)}}$$
$$\times \int_0^{x_{N+1}} \frac{1}{\overline{p}_{\sigma(N)}} e^{-x_N(s+1/\overline{p}_{\sigma(N)})} \ldots \int_0^{x_2} \frac{1}{\overline{p}_{\sigma(1)}} e^{-x_1(s+1/\overline{p}_{\sigma(1)})} dx_1 \ldots dx_L \qquad \text{(A.1)}$$

Recognizing that

$$\sum_{\sigma\in S_N} \int_0^{x_{N+1}} \frac{1}{\overline{p}_{\sigma(N)}} \mathrm{e}^{-x_N(s+1/\overline{p}_{\sigma(N)})} \ldots \int_0^{x_2} \frac{1}{\overline{p}_{\sigma(1)}} \mathrm{e}^{-x_1(s+1/\overline{p}_{\sigma(1)})} dx_1 \ldots dx_N = \prod_{i=1}^{N} \frac{1/\overline{p}_{\sigma(i)}}{s+1/\overline{p}_{\sigma(i)}} \left(1-\mathrm{e}^{-x_{N+1}\left(s+1/\overline{p}_{\sigma(i)}\right)}\right), \qquad \text{(A.2)}$$

we can simplify (A.1) as

$$\phi_I(s) = \sum_{\sigma\in S_L, \sigma(1)<\ldots<\sigma(N)} \int_0^{\infty} \frac{1}{\overline{p}_{\sigma(L)}} e^{-x_L/\overline{p}_{\sigma(L)}} \int_0^{x_L} \frac{1}{\overline{p}_{\sigma(L-1)}} e^{-x_{L-1}/\overline{p}_{\sigma(L-1)}} \ldots \int_0^{x_{N+2}} \frac{1}{\overline{p}_{\sigma(N+1)}} e^{-x_{N+1}/\overline{p}_{\sigma(N+1)}}$$
$$\times \left[\prod_{i=1}^{N} \frac{1/\overline{p}_{\sigma(i)}}{s+1/\overline{p}_{\sigma(i)}} \left(1-\mathrm{e}^{-x_{N+1}\left(s+1/\overline{p}_{\sigma(i)}\right)}\right)\right] dx_{N+1} \ldots dx_L \qquad \text{(A.3)}$$

Note that the product term in (A.3) can be restated as a weighted sum of exponential functions, viz.,

$$\prod_{i=1}^{N} \left(1-e^{x(s+1/\overline{p}_{\sigma(i)})}\right) = \sum_{v=0}^{N} (-1)^v \sum_{b_1+b_2+\ldots+b_N=v} \exp\left[-x\sum_{i=1}^{N} b_i (s+1/\overline{p}_{\sigma(i)})\right] \qquad \text{(A.4)}$$

where $(b_1, b_2, ..., b_N)$ is a binary sequence with each element assuming the value of either 0 or 1. Substituting (A.4) in (A.3) and then interchanging the order of integration, we obtain

$$\phi_I(s) = \sum_{\sigma\in S_{L,N},\sigma(1)<....<\sigma(N)} \left[\prod_{i=1}^{N} \frac{1/\overline{p}_{\sigma(i)}}{s+1/\overline{p}_{\sigma(i)}}\right] \sum_{v=0}^{N} (-1)^v \sum_{b_1+....+b_N=v} \int_0^{\infty} \frac{1}{\overline{p}_{\sigma(N+1)}} e^{-x_{N+1}\left(\frac{1}{\overline{p}_{\sigma(N+1)}}+\sum_{i=1}^{N} b_i (s+1/\overline{p}_{\sigma(i)})\right)}$$

$$\times \left[\int_{x_{N+1}}^{\infty} \frac{1}{\overline{p}_{\sigma(N+2)}} e^{-x_{N+2}/\overline{p}_{\sigma(N+2)}} .... \int_{x_{L-1}}^{\infty} \frac{1}{\overline{p}_{\sigma(L)}} e^{-x_L/\overline{p}_{\sigma(L)}} dx_L ....dx_{N+2}\right] dx_{N+1} \qquad \text{(A.5)}$$

The nested integral identity in (A.5) can be evaluated in closed form using the following integral identity:

$$\sum_{\sigma\in S_N} \int_{x_0}^{\infty} \frac{1}{\overline{p}_{\sigma(1)}} e^{-x_1/\overline{p}_{\sigma(1)}} .... \int_{x_{N-1}}^{\infty} \frac{1}{\overline{p}_{\sigma(N)}} e^{-x_N/\overline{p}_{\sigma(N)}} dx_N ....dx_1 = \prod_{i=1}^{N} e^{-x_0/\overline{p}_{\sigma(i)}} \qquad \text{(A.6)}$$

Thus (A.5) may be restated much more concisely as

$$\phi_I(s) = \sum_{\substack{\sigma\in S_{L,N},\sigma(1)<....<\sigma(N)\\ \sigma(N+2)<....<\sigma(L)}} \left[\prod_{i=1}^{N} \frac{1/\overline{p}_{\sigma(i)}}{s+1/\overline{p}_{\sigma(i)}}\right] \sum_{v=0}^{N} (-1)^v \sum_{b_1+....+b_N=v} \int_0^{\infty} \frac{1}{\overline{p}_{\sigma(N+1)}} e^{-x_{N+1}\left(\frac{1}{\overline{p}_{\sigma(N+1)}}+\sum_{i=1}^{N} b_i (s+1/\overline{p}_{\sigma(i)})+\sum_{i=N+2}^{L} \frac{1}{\overline{p}_{\sigma(i)}}\right)} dx_{N+1}$$

$$= \sum_{\sigma\in T_{L,N}} \sum_{v=0}^{N} (-1)^v \sum_{b_1+b_2+....+b_N=v} \frac{1/\overline{p}_{\sigma(N+1)} \prod_{i=1}^{N} \frac{1/\overline{p}_{\sigma(i)}}{s+1/\overline{p}_{\sigma(i)}}}{\sum_{k=1}^{N} b_k (s+1/\overline{p}_{\sigma(k)}) + \sum_{k=N+1}^{L} 1/\overline{p}_{\sigma(k)}} \qquad \text{(A.7)}$$

where $\sum_{\sigma\in T_{L,N}} = \sum_{\substack{\sigma\in S_L,\sigma(1)<\sigma(2)<...<\sigma(N)\\ \sigma(N+2)<...<\sigma(L)}}$.

Notice that the cardinality of set $T_{L,N}$ is equal to $L!/[N!(L-N-1)!]$ and the total number of summands in (A.7) is $2^N(L-N)\binom{L}{N}$ terms.

Alternatively we can derive yet another closed form expression for $\phi_I(s)$ by restating (5) as (i.e., changing the order of integration of (A.1))

$$\phi_I(s) = \sum_{\sigma\in S_L} \int_0^\infty \frac{1}{\bar{p}_{\sigma(1)}} e^{-x_1(s+1/\bar{p}_{\sigma(1)})} .... \int_{x_{N-1}}^\infty \frac{1}{\bar{p}_{\sigma(N)}} e^{-x_N(s+1/\bar{p}_{\sigma(N)})}$$

$$\times \int_{x_N}^\infty \frac{1}{\bar{p}_{\sigma(N+1)}} e^{-x_{N+1}/\bar{p}_{\sigma(N+1)}} .... \int_{x_{L-1}}^\infty \frac{1}{\bar{p}_{\sigma(L)}} e^{-x_L/\bar{p}_{\sigma(L)}} dx_L ....dx_1 \qquad \text{(A.8)}$$

Using (A.6) in (A.8) and subsequently changing the order of integration, we obtain

$$\phi_I(s) = \sum_{\sigma\in S_L,\sigma(N+1)<....<\sigma(L)} \int_0^\infty \frac{1}{\bar{p}_{\sigma(N)}} e^{-x_N(s+1/\bar{p}_{\sigma(N)}+\sum_{i=N+1}^{L} 1/\bar{p}_{\sigma(i)})}$$

$$\times \left[\int_0^{x_N} \frac{1}{\bar{p}_{\sigma(N-1)}} e^{-x_{N-1}(s+1/\bar{p}_{\sigma(N-1)})} .... \int_0^{x_2} \frac{1}{\bar{p}_{\sigma(1)}} e^{-x_1(s+1/\bar{p}_{\sigma(1)})} dx_1 ....dx_{N-1} \right] dx_N \qquad \text{(A.9)}$$

Next, using identity (A.3) in (A.9), and evaluating the resultant integral, we get a closed form expression for the m.g.f of *I* as

$$\phi_I(s) = \sum_{\sigma\in T_{L,N-1}} \sum_{\nu=0}^{N-1} (-1)^\nu \sum_{b_1+b_2+....+b_{N-1}=\nu} \frac{1/\bar{p}_{\sigma(N)} \prod_{i=1}^{N-1} \frac{1/\bar{p}_{\sigma(i)}}{s+1/\bar{p}_{\sigma(i)}}}{s+\sum_{k=1}^{N-1} b_k(s+1/\bar{p}_{\sigma(k)})+\sum_{k=N}^{L} 1/\bar{p}_{\sigma(k)}} \qquad \text{(A.10)}$$

In this case, the total number of summands in (A.10) is equal to $2^{N-1}N\binom{L}{N}$ because the cardinality of set $T_{L,N-1}$ is $L!/[(N-1)!(L-N)!]$. Therefore, it is apparent that (A.7) is useful for computing $\phi_I(.)$ while $N \geq \lceil L/2 \rceil$ while (A.10) is much more attractive when $N \leq \lfloor L/2 \rfloor$.

Appendix B

In this appendix, we will consider the evaluation of an integral of the form

$$I_r(\beta) = \int_0^\beta \frac{(-1)^r}{\gamma^{r+1}} \phi_o^{(r)}\left(\frac{a}{\gamma}\right) d\gamma \,, r \geq 1, \text{ Re } a > 0 \qquad \text{(B.1)}$$

This integral arises in the computation of outage probability (see (16)), where $\phi_o^{(r)}(c) = \frac{d^r}{ds^r}\phi_o(s)\big|_{s=c}$. Using variable substitution $y = \frac{a}{\gamma}$ in (B.1) we get

$$I_r(\beta) = \int_{a/\beta}^{\infty} \frac{y^{r-1}}{(-a)^r}\phi_o^{(r)}(y)dy \tag{B.2}$$

Next, evaluating (B.2) using integration by parts (by letting $u = y^{r-1}$, $dv = \phi_o^{(r)}(y)dy$, $v = \phi_o^{(r-1)}(y)$), we obtain a recursive formula for computing $I_r(\beta)$, viz..,

$$I_r(\beta) = \frac{(-1)^{r-1}}{a\beta^{r-1}}\phi_o^{(r-1)}\left(\frac{a}{\beta}\right) + \frac{r-1}{a}I_{r-1}(\beta),\ r \geq 2 \tag{B.3}$$

From the above recursion formula it is not very difficult to deduce a non-recursive expression for $I_r(\beta)$ as

$$I_r(\beta) = \frac{\Gamma(r)}{a^r}\sum_{k=0}^{r-1}\frac{1}{k!}\left(\frac{-a}{\beta}\right)^k \phi_o^{(k)}\left(\frac{a}{\beta}\right) \tag{B.4}$$

To the best of the authors' knowledge, (B.4) is new.

Chapter 3

Performance Evaluation of Hybrid Antenna Array Systems in Cellular Mobile Radio Environments

3.1 Chapter Overview

Spectral efficiency in cellular mobile radio environments can be improved by reducing the cochannel reuse distance at the expense of increased cochannel interference level [13]. To reduce the detrimental effects of CCI signals on the reliability of wireless links; cell sectorization, diversity and adaptive interference nulling (AIN) techniques may be employed. Unlike the latter two approaches, cell sectorization reduces the trunking efficiency.

The benefits of AIN is best exploited in an interference hampered environment with a few strong interfering signals (e.g. jammers) where the CCI signal strengths could be much greater than that of the desired user signal. In general, an L - element antenna array can effectively suppress $(L-1)$ of the strongest CCI signals. Diversity reception has long been recognized as an effective technique for mitigating the detrimental effects of multipath fading and cochannel interference. However, it is usually effective in situations where there are many weak CCI signals (i.e., without the presence of strong jammers). As such it is instructive to perform a comparative study between AIN and diversity receiver with a fixed number of antenna elements. This study may provide insights into the selection of the two schemes (or even a combination of both) for a specified dimension of an antenna array.

For instance, increasing the number of antenna elements L indefinitely does not provide a considerable performance improvement for MRC (since the relative diversity improvement diminishes with increasing diversity order) but it is very effective for AIN as more CCI signals can be suppressed. Also, diversity schemes rely on the statistical independence of the received signals to achieve diversity improvement. Thus, spatial

diversity schemes exploit the possibility of realizing a low fading correlation by increasing the spacing between antenna elements (e.g. approximately $\lambda/2$ at a mobile handset and in the order of 10-20λ for a base-station; λ is the operating frequency wavelength). In AIN on the other hand, the antenna element spacing is constrained to $\lambda/2$ (Nyquist spacing) or less. The faded distribution of the desired user signal also has an impact on the selection between AIN and MRC.

By now, it should be apparent that the choice between AIN and MRC (or EGC) schemes in a specified operating environment is not obvious. This lays an open question: "Given an antenna array with L elements, which is better in a cellular mobile radio environment: MRC (or EGC), AIN or hybrid AIN/MRC?" This chapter makes an attempt to provide a partial answer to the above fundamental question by developing a mathematical framework for analyzing a hybrid AIN/MRC scheme, where D out of L elements will be utilized for AIN of dominant interferers while the remaining $L - D$ elements will be used for diversity combining. For the purpose of illustration we shall confine ourselves to the Nakagami-m faded desired user signal statistic and independent and identically distributed (i.i.d) Rayleigh faded CCI signals. Although it is possible to relax the assumptions and extend the analysis to a generalized fading environment, this treatment is beyond the scope of this discussion.

Next, we provide a brief literature review of related published work. In [17], the authors studied the outage probability performance of diversity cellular systems with cochannel interference in Nakagami-m fading. Ref. [18] examined the effect of CCI signals on the average error probability performance of binary signaling schemes in a Nakagami-m fading environment. Extensive analysis of the AIN scheme is carried out in [7]-[8] for i.i.d Rayleigh faded CCI signals and in [9] for i.i.d Nakagami-m CCI signal statistics.

3.2 SIR Statistics

In this section we first derive a generic solution for the probability density function (p.d.f) of the SIR. Subsequently a closed form expression for the p.d.f is derived for the case where the CCI signals are Nakagami-m faded, while the desired user signal could follow

any arbitrary fading distribution. In an interference-limited environment the SIR is given by $\gamma = p_d / I$, where the random variables p_d and I correspond to the desired user signal power and the total power of all cochannel interferers respectively. The p.d.f in this case can be expressed as

$$f_\gamma(\gamma) = \int_0^\infty x f_d(\gamma x)\, f_I(x) dx \tag{1}$$

The above expression can be restated in terms of the moment generating function (m.g.f) of the desired user and CCI signals, viz.,

$$f_\gamma(\gamma) \cong \frac{-4}{T\gamma^2} \sum_{\substack{n=1 \\ n\ odd}}^{\infty} \mathrm{Re}\left[\phi_I\left(\frac{-j2\pi n}{T}, N_I - D + 1 \right) \phi_d^{(1)}\left(\frac{j2\pi n}{T\gamma}, L - D + 1 \right) \right] \tag{2}$$

where $\phi_d^{(1)}\left(\frac{j2\pi n}{T\gamma}, L - D + 1 \right)$ represents the first order derivative of the m.g.f for the desired user signal with $(L - D + 1)$ diversity branches, N_I is the number of CCI signals, L is the diversity order of the antenna array system, D denotes the number of antenna elements used for adaptive interference nulling and ($N_I - D + 1 = N$) is the number of uncancelled interferers (residual interferers after successive interference cancellation). The expression in (2) can be used to study the effect of cochannel interferers with MRC, adaptive interference nulling and the hybrid AIN/MRC scheme. Subsequent subsections would look into each scheme in detail and provide a mathematical framework for evaluating the performance of the antenna array system employing such schemes.

3.2.1 MRC Diversity Combining (D =1)

For the limiting case of $D = 1$, Eq. 2 reduces to a pure diversity combining receiver. In order to evaluate the performance of the MRC receiver, we require the knowledge of the p.d.f and m.g.f of the SIR. While the CCI signals are Nakagami-m faded we can obtain a closed form solution for the p.d.f, viz.,

$$f_{\gamma(MRC)}(\gamma) = \frac{1}{\Gamma(m_i N_I)} \left(\frac{-m_i}{p_i \gamma} \right)^{m_i N_I} \frac{1}{\gamma} \phi_d^{(m_i N_I)}\left(\frac{m_i}{p_i \gamma}, L \right) \tag{3}$$

where m_i is the fading index and $\bar{p}_i$ the average power of the CCI signals. The factor $\phi_d^{(m_i N_I)}\left(\frac{m_i}{\bar{p}_i \gamma}, L\right)$ is of the form $\phi_d^{(n)}(s, L)$, the *n*-th order derivative of the m.g.f of the desired user signal summarized in Table 1. It is worth noting, that Eq. (3) holds good for arbitrary fading distribution of the desired user signal as long as $m_i N_I$ is a positive integer. However for the specific case of Nakagami-m faded desired user signal a slightly more general expression is given in [18] which holds for arbitrary m_i. It is also worthwhile to derive a closed form solution for the m.g.f of the SIR. Although (3) holds for arbitrary desired user signal statistics, the m.g.f can be evaluated in closed-form only for the special case of Nakagami-m faded desired user signal. The p.d.f in (3) for this case can be restated as

$$f_{\gamma(MRC)}(\gamma) = \frac{\Gamma(m_d L + m_i N_I)}{\Gamma(m_d L)\Gamma(m_i N_I)} \gamma^{m_d L - 1} \left(\frac{m_d}{\bar{m_i \gamma}}\right)^{m_d L} \left(1 + \frac{m_d \gamma}{\bar{m_i \gamma}}\right)^{-m_d L - m_i N_I} \tag{4}$$

Using (4) a closed form solution for the m.g.f can be derived in terms of the confluent hypergeometric function of the second kind, yielding

$$\phi_{\gamma(MRC)}(s, L) = \frac{\Gamma(m_d L + m_i N_I)}{\Gamma(m_i N_I)} U\left(m_d L, 1 - m_i N_I, \frac{\bar{m_i \gamma s}}{m_d}\right) \tag{5}$$

where the function *U (a; b; z)* can be easily evaluated using the generalized hypergeometric function given by [14, (Eq. 13.1.10)] available in standard software packages such as MATLAB

$$U(a, b, z) = z^{-a}\, {}_2F_0(a, 1 + a - b; ; -1/z) \tag{6}$$

It should be highlighted here that the expression for the m.g.f of the SIR derived in (5) follows a simpler analysis than the one carried out in [18].

3.2.2 Adaptive Interference Nulling (D = L)

For the limiting case of *D = L*, an adaptive null steering algorithm can be employed for evaluating the performance of antenna array systems. In this case the first order derivative of the m.g.f of the desired user signal corresponds to that of a single diversity

branch (See Eq. (2)). Using the p.d.f of the sum of uncancelled interfering signals $f_I(.)$, the authors in [19] have derived a closed form solution for the p.d.f of the SIR (when the CCI signals are Nakagami-m faded). Subsequently utilizing the p.d.f statistics, closed form solutions for the m.g.f of the SIR were also derived.

For the purpose of illustration we consider the case where the CCI signals are Rayleigh faded and the desired user signal is subjected to Nakagami-m fading. The m.g.f of the SIR can be expressed as

$$\phi_{\gamma(AIN)}(s) = \binom{N_I}{N} \sum_{n=1}^{N} (-1)^{n-1} \left(\frac{(N-n+1)^N m_d}{(N_I - N)^{N-1}(N_I - n + 1)} \right)$$

$$\times \binom{N}{n-1} \Gamma(m_d) U\left(m_d, 0, \frac{-s\bar{\lambda}(N_I - n + 1)}{m_d(N - n + 1)} \right) \qquad (7)$$

This equation originally derived in [20] is restated here for the convenience of the reader.

3.2.3 Hybrid AIN / MRC (1 < D < L)

An analytical framework for characterizing the performance of cellular mobile radio systems employing either an adaptive null steering algorithm or a diversity combining receiver were developed in the previous sections. It is also possible to analyze the case of a hybrid AIN/MRC receiver. Probability of outage as well as the ASER for the hybrid case can be effectively studied and requires the knowledge of the m.g.f of the SIR alone. The m.g.f of the SIR for an antenna array system employing a hybrid AIN/MRC scheme can be expressed as

$$\phi_{\gamma(hybrid)} = \phi_{\gamma(AIN)}(N_I - D + 1)\phi_{\gamma(MRC)}(L - D + 1) \qquad (8)$$

As an example, consider the case of a six-element antenna array (L = 6), the various synergistic possibilities of selecting either AIN or MRC diversity combining or even a combination of both is shown in Table 3-1.

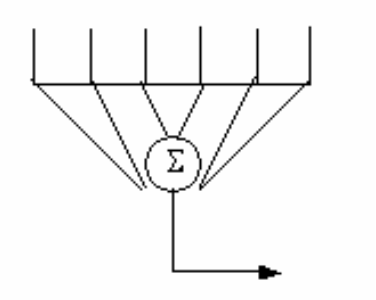 $D=1,\ \phi_{\gamma(MRC)}(s,6)$	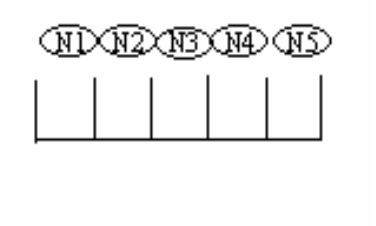 $D=L,\ \phi_{\gamma(AIN)}(s,N_I-5)$
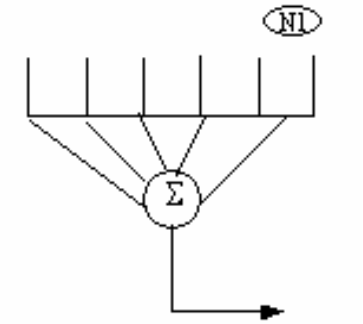 $D=2,\ \phi_{\gamma(MRC)}(s,5)\phi_{\gamma(AIN)}(s,N_I-1)$	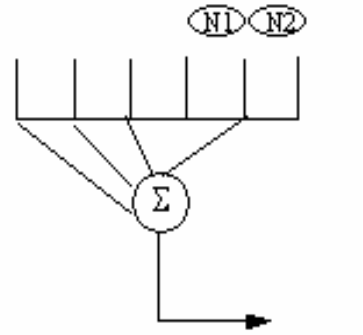 $D=3,\ \phi_{\gamma(MRC)}(s,4)\phi_{\gamma(AIN)}(s,N_I-2)$
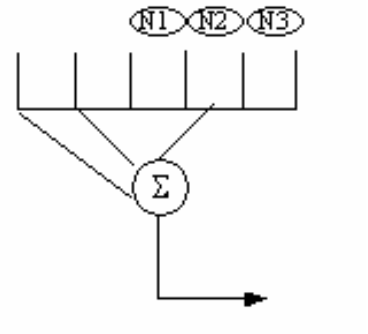 $D=4,\ \phi_{\gamma(MRC)}(s,3)\phi_{\gamma(AIN)}(s,N_I-3)$	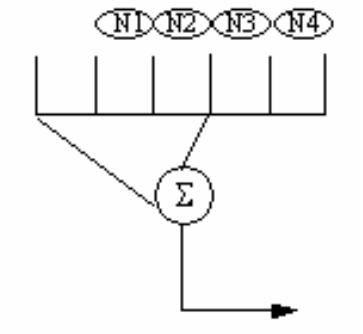 $D=5,\ \phi_{\gamma(MRC)}(s,2)\phi_{\gamma(AIN)}(s,N_I-4)$

Table 3-1 Hybrid AIN/MRC scheme for the case of six antenna elements

3.3 Outage Analysis

The probability of outage is an important statistical measure for the performance evaluation of cellular mobile radio systems in the presence of CCI. In an environment limited by cochannel interference satisfactory reception is achieved as long as the short term SIR exceeds the CCI power protection ratio *q*. The outage event can be expressed as

$$P_{out} = P\left(\gamma = \frac{p_d}{p_I} < q\right) = \int_0^q f_\gamma(\gamma)d\gamma \tag{9}$$

A generalized expression for the probability of outage that holds for all cases discussed in Section II is given by

$$P_{out} \cong \frac{2}{j\pi}\sum_{\substack{n=1 \\ n\ odd}}^{\infty}\frac{1}{n}\mathrm{Re}\left[\phi_I\left(\frac{-j2\pi n}{T}, N_I - D + 1\right)\phi_d\left(\frac{j2\pi n}{T\gamma_{th}}, L - D + 1\right)\right] \tag{10}$$

3.3.1 Case D = 1

For an MRC receiver the outage probability can be obtained in closed-form by substituting (3) into (9). The final expression is given by

$$P_{out(MRC)} = \sum_{k=0}^{m_i N_I - 1}\frac{1}{k!}\left(\frac{-m_i}{p_i q}\right)^k \phi_d^{(k)}\left(\frac{m_i}{p_i q}, L\right) \tag{11}$$

The closed form solution in (11) holds for the case of Nakagami-m faded CCI signals. Utilizing the n-th order derivative of the m.g.f summarized in Table. 1, (11) can be computed for arbitrary fading distributions of the desired user signal.

3.3.2 Case D = L

Extensive analysis on the probability of outage for adaptive interference nulling is available in [7]-[9] and [19]-[20]. In [11] and [21] the authors have derived a generalized expression for the outage probability that holds for all common fading distributions for both the desired user signal as well as the CCI signals (See Eq. (10) in [21]). Since closed-form solution for the desired user signal for all fading distributions is available, we require the knowledge of the m.g.f of the sum of uncancelled interfering signals $\phi_I(.)$ alone. Following this ([9], Eq. (A2)) derived an expression for $\phi_I(.)$ which holds for all fading distributions. But the probability of outage can be computed in closed form only for the special case of Nakagami-m faded CCI signals. Closed-form solutions for this case is presented in ([9], Eqs. (19)-(21)).

3.3.3 Case (1 < D < L)

An alternate way for computing the outage probability using the m.g.f of the SIR is presented in this subsection. The outage probability for the hybrid AIN/MRC scheme can be easily computed by using the Laplace inversion method suggested in [22]. Utilizing (8) the outage probability for the hybrid AIN/MRC scheme can be computed using the following expression

$$P_{out} = \sum_{c=0}^{C} 2^{-C} \binom{C}{c} \left[\frac{e^{A/2}}{x} \sum_{b=0}^{B+c} \frac{(-1)^b}{\alpha_b} \Re\left\{ \frac{2x}{(A+2\pi ib)} \phi_\gamma \left(\frac{A+2\pi ib}{2x} \right) \right\} \right] \tag{12}$$

where $\alpha_0 = 2$, $\alpha_b = 2$ for any $b \geq 1$, $\Re\{.\}$ denotes the real part of the complex argument and the constants *A, B, C* are arbitrarily chosen to be 30, 18 and 24 respectively, to yield an accuracy of at least 10^{-6}.

3.3.4 Numerical Results

To illustrate the utility of the outage expressions derived in this section we present probability of outage plots for MRC diversity combining as well as the hybrid scheme. Figure 3-1 depicts the normalized SIR versus probability of outage curves when the desired user signal is Rician distributed. We observe that with a receiver employing diversity combining the outage probability decreases as the diversity order is considerably increased. However, the *relative* outage gain with MRC diminishes with increasing diversity order. We also see that an MRC receiver works best at higher SIR/q regions where the system is noise limited.

Figure 3-2 plots the normalized SIR versus probability of outage curves for the hybrid AIN/MRC scheme. We observe that with an *L* element antenna array, pure AIN works best at lower SIR/q regions. On the other hand a pure diversity combining receiver performs best at higher SIR/q values. The hybrid schemes tend to perform in the direction in which either of the two schemes is dominant. For example the hybrid receiver *D = 2* in which four out of six antenna elements are used for diversity combining and the remaining two are used for the canceling of dominant interferers (AIN), works best at

higher SIR/q regions. In contrast an hybrid receiver with $D = 4$, in which two out of the six elements are used for diversity combining and the remaining four are used for canceling of dominant interferers (AIN), works best at lower SIR/q regions where the system is interference limited. The fact that more number of elements is being employed for null steering would obviously improve system performance at this operating region.

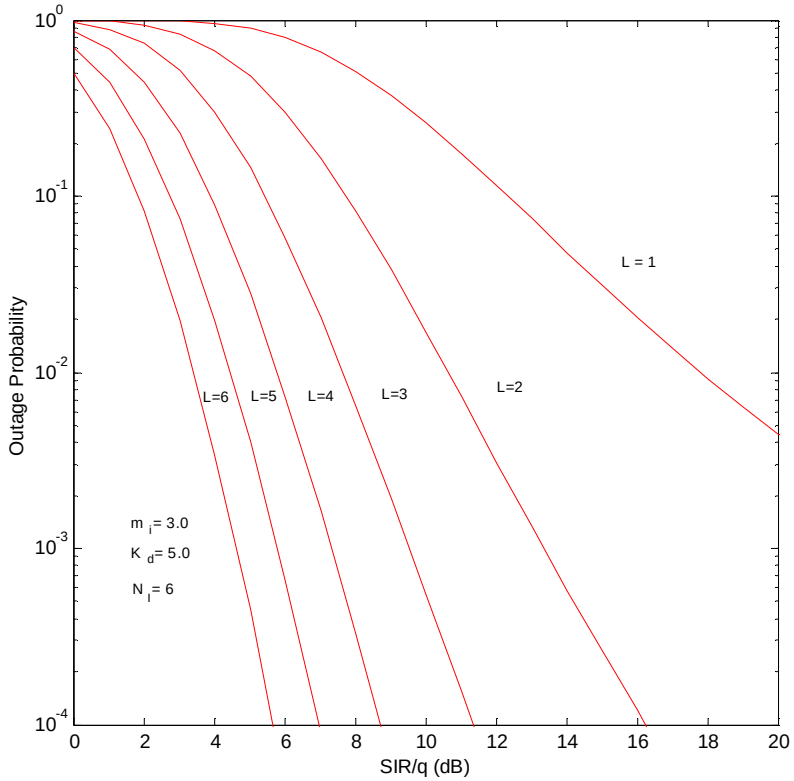

Figure 3-1 Outage probability versus average SIR/q for MRC diversity cellular system in the presence of Nakagami-m faded CCI signals; the desired user follows Rician distribution

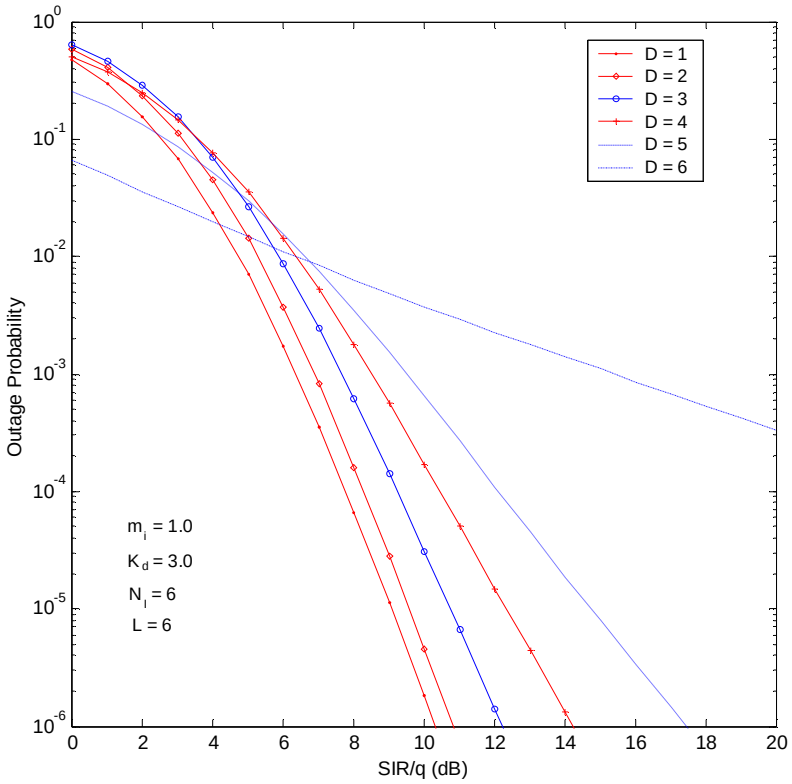

Figure 3-2 Outage probability versus average SIR/q for the hybrid AIN/MRC scheme in the presence of Rayleigh faded CCI signals; the desired user follows Rician distribution

3.4 ASER Analysis

The ASER for different digital modulation schemes can be easily computed using either the p.d.f or the m.g.f approach. The ASER using the p.d.f of the SIR can be expressed in terms of the conditional error probability $P_s(\gamma)$ and is given by

$$\overline{P}_s = \int_0^\infty P_s(\gamma)\, f_\gamma(\gamma)\, d\gamma \tag{13}$$

It is worth noting, that the presence of a closed-form solution for the p.d.f of the SIR in (3) provides an easy way of computing the ASER utilizing the single integral expression in (13). Alternatively the ASER can be computed using the m.g.f approach. This is investigated in the following subsections.

3.4.1 Coherent Receiver

Coherent receivers work best under slow time variations of the channel and require a lower SIR to meet a fixed average error probability. The ASER for both coherent and non-coherent modulation schemes can be easily computed using the argument of the m.g.f. The ASER of M_c - PSK can be computed using the following expression

$$\overline{P}_s = \frac{1}{\pi} \int_0^{\pi - \pi/M_c} \phi_\gamma \left(\frac{\sin^2(\pi / M_c)}{\sin^2 \theta} \right) d\theta \tag{14}$$

where M_c denotes the alphabet size of M-ary signal constellations. The ASER for M-ary DPSK can be computed using

$$\overline{P}_s = \frac{1}{\pi} \int_0^{\pi - \pi/M_c} \phi_\gamma \left(\frac{\sin^2(\pi / M_c)}{1 + \cos(\pi / M_c)\cos\theta} \right) d\theta \tag{15}$$

3.4.2 Non-coherent Receiver

Consider the case of a fast moving mobile user; in such a situation it is difficult to get an accurate channel estimate at the receiver. The use of post-detection equal-gain combining (non-coherent detection schemes) in such a scenario circumvents the need to co-phase and weight the diversity branches. The average bit error probability for π/4-DQPSK with non-coherent receiver can be computed using

$$\overline{P}_b = \frac{1}{(1+\eta)^{2L-1} 2\pi} \int_0^{2\pi} \frac{g(\theta)}{1 - 2\beta\cos\theta + \beta^2} \phi_\gamma \left[\frac{b^2}{2} (1 - 2\beta\cos\theta + \beta^2) \right] d\theta \tag{16}$$

where $0^+ < \beta = a/b < 1$,

$$g(\theta) = \sum_{k=0}^{2L-1} \binom{2L-1}{k} \beta^{k+1-L} \eta^k \{\cos[(k-L+1)\theta] - \beta\cos[(k-L)\theta]\} \tag{17}$$

and the constants a = $\sqrt{2 - \sqrt{2}}$, $b = \sqrt{2 + \sqrt{2}}$ and $\eta = 1$.

It is instructive at this point to make a comparative study of the advantages of using either the p.d.f or the m.g.f approach depending on their computational complexity. As highlighted before, the use of the p.d.f approach is appropriate when the p.d.f of the SIR is available in closed form, as in such a situation the error rates can be computed using a

single integral expression. However, the existence of the m.g.f of the SIR in closed-form while the desired user signal is Nakagami-m faded extends the utility of the m.g.f approach, as it is possible to compute the ASER in this case for a myriad of digital modulation schemes.

3.4.3 Numerical Results

Selected numerical results for the ASER are presented in this section. Figures 3-3 and 3-4 show the average SIR versus the average error probability curves with MRC in a Nakagami-m fading environment. We observe an appreciable performance gain with increasing diversity order. However, the relative diversity gain diminishes with increasing *L*. The performance of coherent DQPSK in Figure 3-3 is marginally better compared to its non-coherent counterpart, it should be highlighted however, that the non-coherent receiver structure does not require phase information and is beneficial in situations where channel variations are rapid.

Figure 3-5 depicts the average SIR versus ABER curves for DPSK modulation with a hybrid AIN/MRC scheme. We observe that AIN works best at lower SIR regions, whereas MRC diversity combining outperforms AIN at higher average SIR. The hybrid schemes exploit the best of both worlds; they tend to perform in the direction in which either of the two schemes is dominant. For example the hybrid receiver $D = 2$ in which four out of six antenna elements are used for diversity combining and the remaining two are used for the canceling of dominant interferers (AIN), works best at higher SIR/q regions. In contrast an hybrid receiver with $D = 4$, in which two out of the six elements are used for diversity combining and the remaining four are used for canceling of dominant interferers (AIN), works best at lower SIR/q regions where the system is interference limited. The fact that more number of elements is being employed for null steering would obviously improve system performance at this operating region.

Figure 3-6 plots the ABER versus the number of CCI signals for DPSK modulation at an operating SIR of 10 dB. It is apparent from the figure that MRC works best when the

number of CCI signals is small, however even in an interference-hampered environment an appreciable gain can be realized by increasing the diversity order.

3.5 Conclusion

This chapter presented an analytical framework for characterizing the performance of a hybrid AIN/MRC scheme in a cellular mobile radio environment in terms of the outage probability and average symbol error rate. Generic expressions for the p.d.f and c.d.f of the SIR at the output of a hybrid AIN/MRC receiver are derived. The expressions derived in this chapter are sufficiently general and can also be used for studying the performance of an AIN alone or an MRC alone receiver as limiting cases. Selected design examples are provided to show the benefits of employing a hybrid AIN/MRC receiver for cellular mobile radio communications. Given constraints over the number of antenna elements that can be employed at the mobile handset the use of a hybrid AIN/MRC receiver is an attractive option. The trade-offs between these two schemes in terms of the length of antenna array, antenna spacing, fading correlation of the signals etc., provide a further impetus to employ such a receiver. Finally, the results obtained in this research answer to a great extent the selection of either schemes or even a combination of both depending on the cellular mobile radio environment in which they are to be deployed.

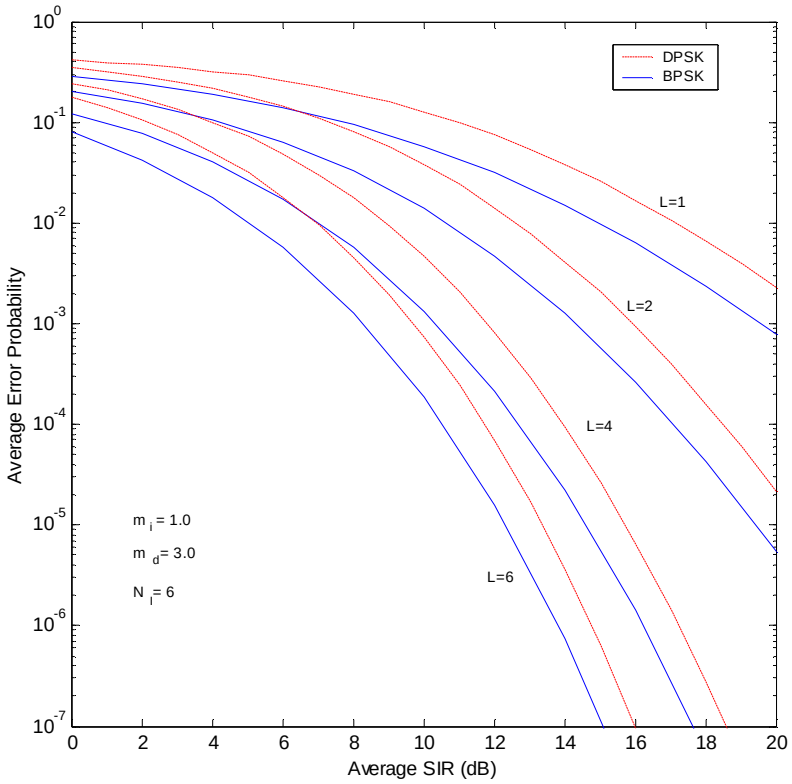

Figure 3-3 Average error probability versus SIR for DPSK modulation in the presence of Rayleigh faded CCI signals; the desired user is Nakagami-m fading

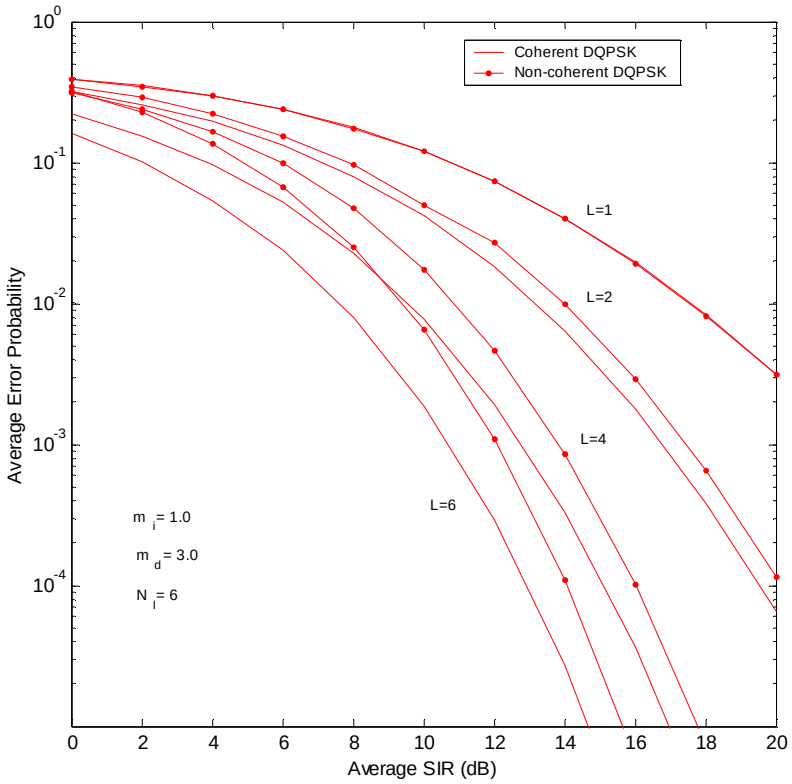

Figure 3-4 Average error probability versus average SIR for coherent and non-coherent DQPSK modulation in the presence of Rayleigh faded CCI signals; the desired user follows Nakagami-m fading

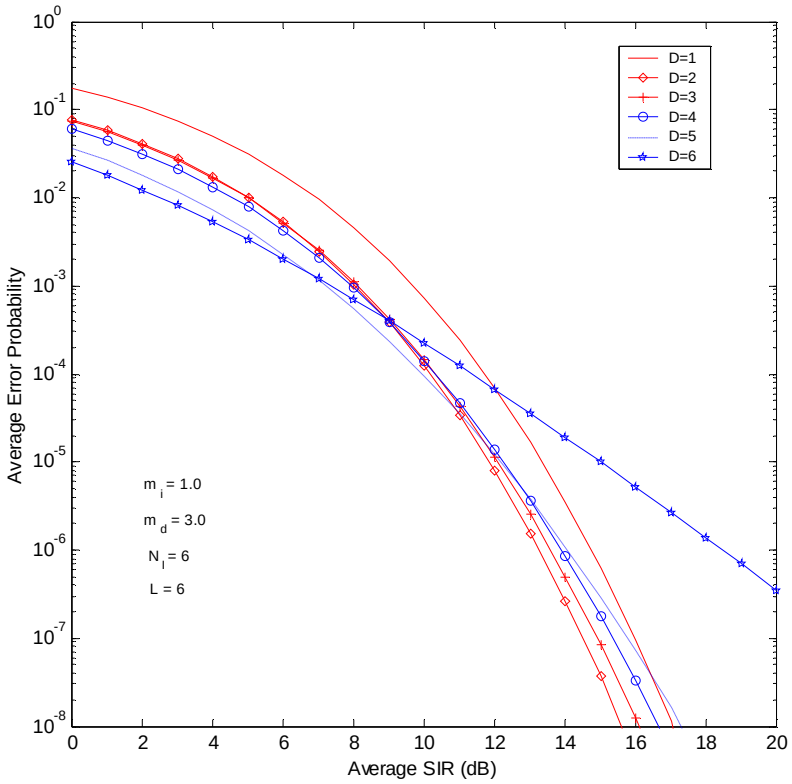

Figure 3-5 Average error probability versus average SIR for the hybrid AIN/MRC scheme with DPSK modulation in the presence of Rayleigh faded CCI signals; the desired user follows Nakagami-m fading

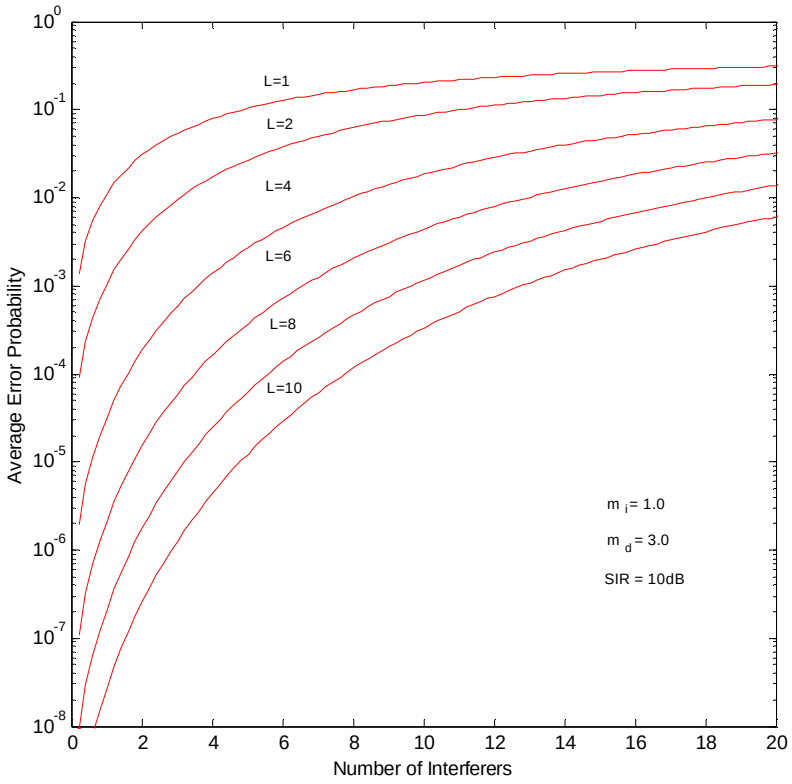

Figure 3-6 Average error probability versus number of interferers for DPSK modulation in the presence of Rayleigh faded CCI signals; the desired user is Nakagami-m faded

Chapter 4

Adaptive MAC Scheduling in Wireless Networks

4.1 Goals and Objectives

The primary goal of this work is to show the performance gains possible, by exploiting the synergy resulting from the combination of the MAC and the physical layer. In this case, the adaptive physical layer (variable rate encoder and modulation) provides CSI to the transmitter through a low-capacity feedback channel. For good channel conditions the amount of error protection to be added at the transmitter is reduced, thus increasing the throughput. On the other hand when the channel condition deteriorates, the amount of error protection is increased. This mechanism, in which the coding rate and the modulation scheme are changed adaptively according the nature of the channel helps in maintaining a constant throughput. The proposed, synergistic use of the MAC and the physical layer increases the fidelity of cross-layer simulations. Specifically, two different kinds of cross-layer simulation approaches are investigated as part of this research:

- Baseline System (Fixed rate channel encoder)
- Full PHY-MAC layer simulation, System (adaptive channel encoder with MAC interaction)

In the Baseline System a dynamic time division multiple access (DTDMA) based MAC layer is implemented with a fixed rate channel encoder. The schematic diagram of such a model is shown in Figure 4-1. The entire system model will be described in more detail in the later part of this chapter.

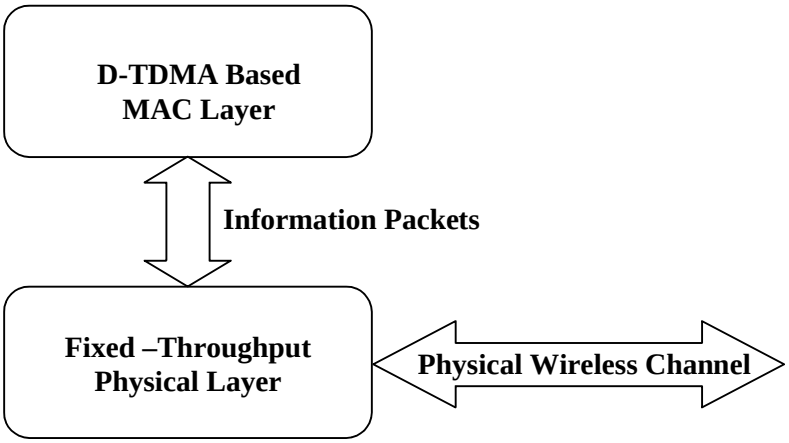

Figure 4-1 Baseline System: Fixed Rate Channel Encoder without PHY and MAC layer interaction

Full PHY-MAC layer system with a variable rate channel encoder and MAC interaction is shown in Figure 4-2. This system implements a DTDMA based MAC layer along with a variable rate channel encoder which is responsible for switching between one of three available transmission modes depending on the channel condition, or more specifically, the estimated BER value. As expected, the novel design of the full PHY-MAC layer system outperforms the Baseline system and is hence an obvious choice for cross-layer design.

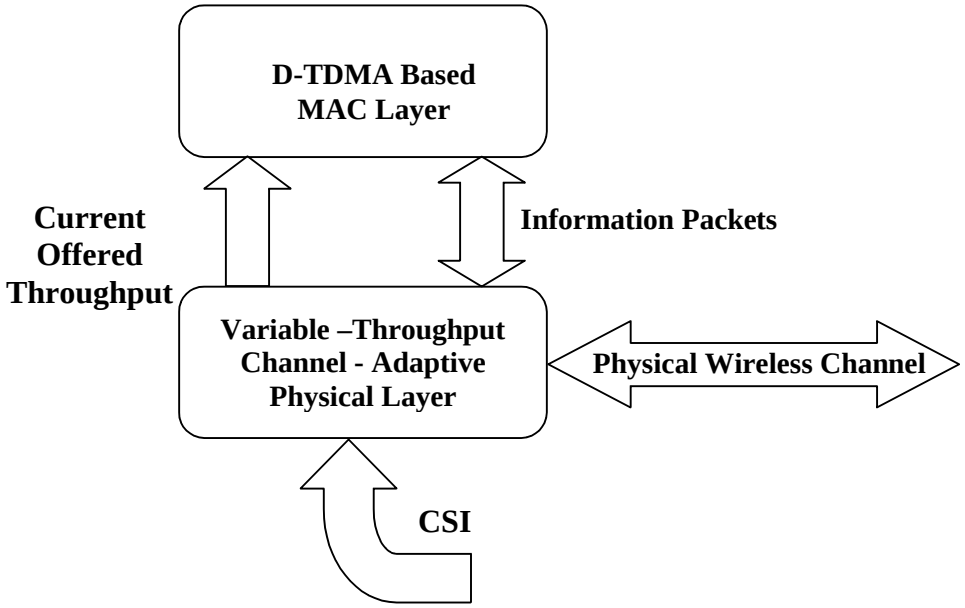

Figure 4-2 CSI Dependent MAC System–II: Adaptive Channel Encoder with MAC Interaction

A co-simulator using MATLAB for modeling the physical layer is used for this project. The two approaches described in this section are compared for fidelity. For fidelity, the full PHY-MAC layer system is the benchmark as it incorporates all the parameters described in this chapter.

4.2 System Description

This section provides an overview of the system chosen to demonstrate the approaches developed in this research including a detailed description of the physical layer [23]-[24].

4.2.1 Physical Layer Description

A complete physical layer simulator based on the IEEE 802.11a standard [25] is used in the cross-layer simulations. OFDM is selected as the modulation of choice to combat frequency selective fading and to randomize the burst errors caused by a wideband fading channel. The key parameters of the OFDM standard used in the physical layer simulation are illustrated in Table 4-1 [25]-[26].

Parameter	**Value**
Data Rate	**6, 9, 12, 18, 24, 36, 48, 54 Mbps**
Modulation	**BPSK, QPSK, 16-QAM**
Coding Rates	**1/2, 2/3, ¾**
Number of Subcarriers	**52**
Number of Pilot Tones	**4**
OFDM Symbol Duration	**4 μsec**
Subcarrier Spacing	**312.5 kHz**
Signal Bandwidth	**16.66 MHz**
Channel Spacing	**20MHz**
Guard Interval	**800 ηsec, 400 ηsec**

Table 4-1 Key Parameters of the OFDM Simulator developed in MATLAB based on the 802.11a standard

Note that the selection of the transmission rate is determined by a link adaptation scheme, *i.e.*, a process of selecting the best coding rate and modulation schemes based on channel conditions. Preparation for transmission and data recovery are performed by the block diagram shown in Figures 4-3 and 4-4.

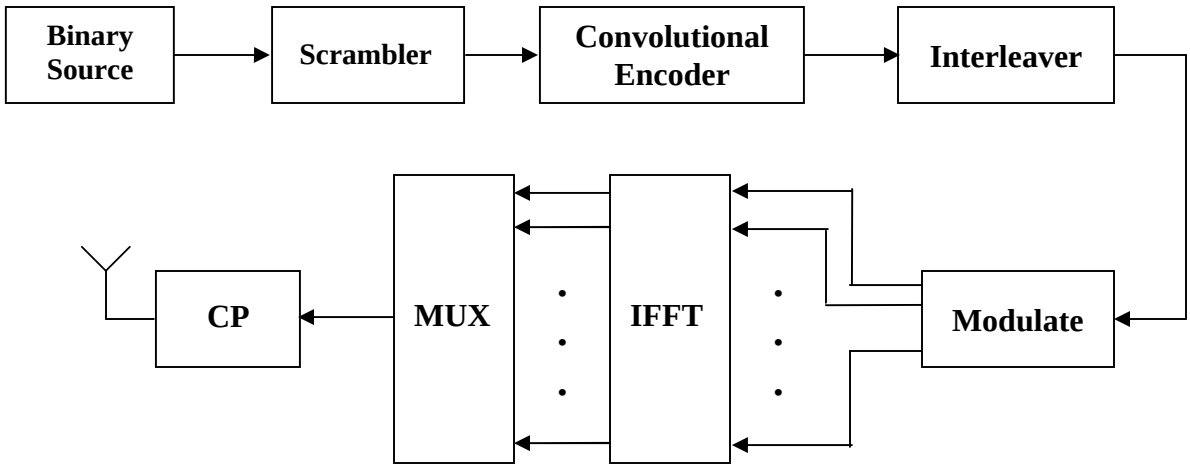

Figure 4-3 A Simplified Block Diagram of an IEEE 802.11a Transmitter

4.2.1.1 OFDM Signal Generation

The sequence of steps that lead to OFDM signal generation is illustrated next. The binary source generates random digits that are passed through a scrambler. The purpose of the scrambler is to prevent a long sequence of 1's and 0's. Next, the scrambled data sequence is encoded with a (2, 1, 7) convolutional encoder. The other coding rates are obtained by puncturing the parent code at the output of the encoder. Three different coding rates are generated by using different puncturing patterns. Puncturing involves the deletion of coded bits from the output data sequence such that the ratio of coded bits (k) to the uncoded bits (n), (i.e., k/n) is greater than the parent code [27]. For example, to achieve a code rate of 2/3, one bit out of every four bits is deleted from the coded sequence.

Following the puncturing operation, the coded bits are interleaved to prevent any burst errors. The interleaved coded bits are then grouped together to form symbols. Specifically three modulation schemes are implemented in the simulator (see Table 1). Next, the modulation symbols are mapped to the subcarrier of the 64-point IDFT, to create the OFDM symbol. A total of 52 subcarriers are used of which 48 subcarriers are used for data modulation and the remaining 4 subcarriers are used as pilot symbols. The pilot

symbols are used in the downlink for estimating the channel state information on the basis of which scheduling is done. After the IDFT operation a cyclic prefix (CP) is added to the OFDM symbols. The resulting signal is then transmitted across the channel. A final note, as long as the duration of the CP is longer than the channel impulse response, ISI will be eliminated.

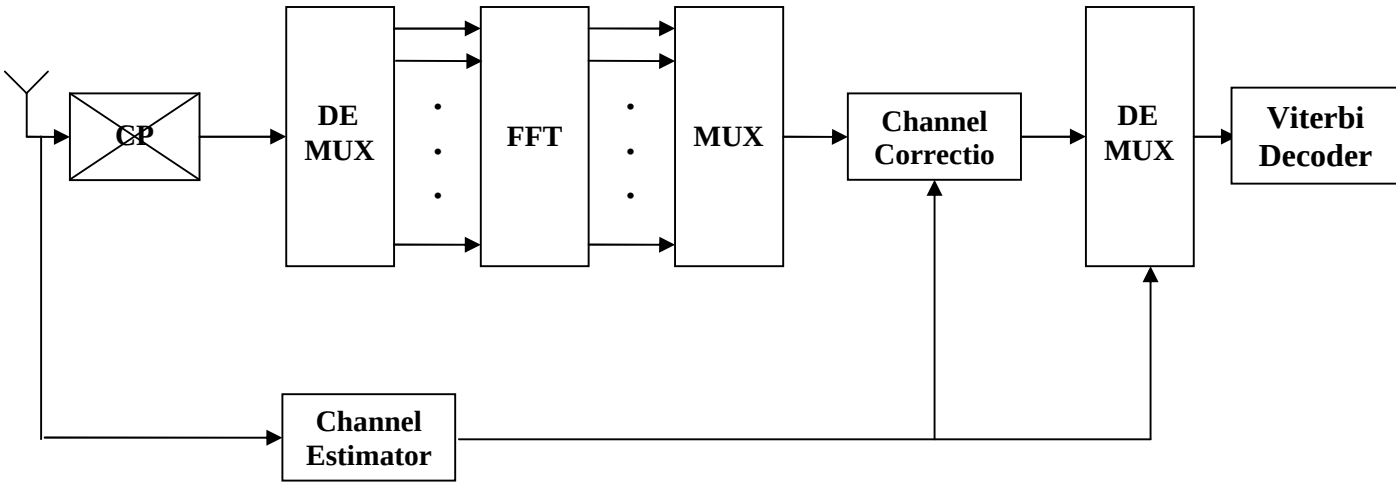

Figure 4-4 A Simplified Block Diagram of an IEEE 802.11a Receiver

4.2.1.2 OFDM Signal Reception

At the receiver the CP is first removed, following which the receiver performs the inverse operations of the transmitter. Before any receiver algorithms can be employed, the timing clock at the receiver must be synchronized with that of the transmitter. This is done by using the data aided time domain frequency synchronization algorithm [28]. Another important aspect of the OFDM receiver is channel estimation that is required to demodulate the symbols. Two different training sequences are provided: short and long training sequences. The short training sequence is used to provide coarse and fine estimation of time and frequency errors. The long training sequences are used to estimate the channel impulse response or CSI. With the CSI, the received signal can demodulated, deinterleaved, and input to the Viterbi algorithm for decoding.

4.2.1.3 Variable Rate Channel Encoder

Two important blocks of the OFDM transceiver that require a more detailed description are addressed next. These include the variable rate channel encoder and the channel model itself. These hold the key for the scheduling algorithms that would be discussed in the following sections.

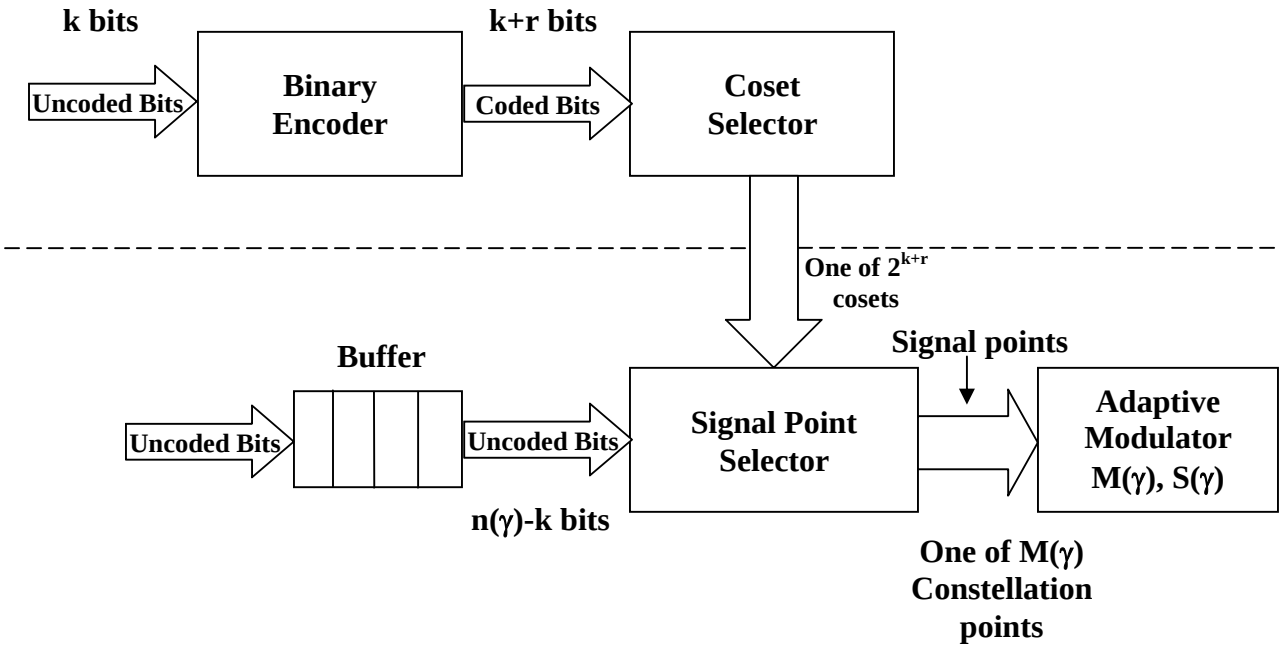

Figure 4-5 A variable rate channel encoder providing three transmission modes, varying modulation scheme and coding rates

The general structure of an adaptive coded modulation is shown in Figure 4-5. Specifically, a binary encoder operates on k uncoded bits to produce $k + r$ coded bits, and the coset selector uses these coded bits to select one of the 2^{k+r} cosets from a partition of the signal constellation. The basic premise for using adaptive modulation with coset codes is to keep these distances constant by varying the size of the signal constellation. By maintaining a constant minimum distance the adaptive modulation exhibits the same coding gain as coded modulation for an AWGN channel with minimum coded distance

d_{min} [29]. The adaptive modulator of Figure 4-5 is used in our physical layer simulator. The modulator would specifically switch between BPSK, QPSK and 16-QAM with respect to variations in channel conditions.

4.2.1.4 Rayleigh Channel Model

This section, investigates a channel model that predicts the effect of multipath on the transmitted signal. The baseband transmit signal s(t) can be modeled as a narrowband process related to the information bearing signal x(t) as (1)

$$s(t) = x(t)e^{-j2\pi f_c t} \tag{1}$$

Under the assumptions of Gaussian scatters and multiple propagation paths to the receiver, the channel is characterized by time-varying propagation delays, attenuation factors, and Doppler shifts. In [30] it is shown that the time variant impulse response is given by (2)

$$c(\tau_n, t) = \sum_n \alpha_n(\tau_n(t))e^{-j2\pi f_{D_n}\tau_n(t)}\delta\left[t - \tau_n(t)\right] \tag{2}$$

where

$c(\tau_n, t)$ is the response of the channel at time *t* due to an impulse applied at time $t - \tau_n(t)$

$\alpha_n(t)$ is the attenuation factor for the received signal on the n^{th} path

$\tau_n(t)$ is the propagation delay for the n^{th} path

f_{D_n} is the Doppler shift for the signal received on the n^{th} path

Therefore, the output of the channel is simply the convolution of (1) and (2) and can be expressed as (3)

$$\begin{aligned} z(t) &= c(\tau_n, t) * s(t) \\ &= \sum_n \alpha_n(\tau_n(t))e^{-j2\pi(f_c + f_{D_n})\tau_n(t)} x\left[t - \tau_n(t)\right]e^{-j2\pi f_c t} \end{aligned} \tag{3}$$

Notice that the envelope of $c(\tau_n, t)$ at any instant *t*, exhibits a Rayleigh distribution since it is the sum of Gaussian random processes.

4.2.2 MAC Layer Description

This section first looks into some properties a scheduling algorithm should possess, followed by a conventional design for a wireless scheduler. For the latter part, a brief description of the implemented scheme is provided.

It is in most cases desirable for a scheduling algorithm to possess the following features [31]-[34]:

- *Efficient Link Utilization*: The scheduling algorithm must be able to utilize the channel efficiently. This means that the scheduler should assign time slots to those users with good channel states and delay the requests of those users with bad CSI.
- *Fairness*: The algorithm should be able to redistribute available resources fairly among sessions. It should provide fairness among error free sessions and error prone sessions that is short term and long term fairness respectively.
- *Throughput*: The algorithm should be able to provide guaranteed short term throughput among error free sessions and guaranteed long term throughput among all sessions

Figure 4-6 shows the schematic of a typical wireless scheduler [35]. Here scheduling is done at the base station, which can communicate with all mobile stations. Typically scheduling is done for the downlink, based on channel state information sent by the mobile through a feedback channel. For this research a similar wireless scheduler was implemented with a fully functional physical layer simulator in MATLAB and a DTDMA based MAC layer in OPNET.

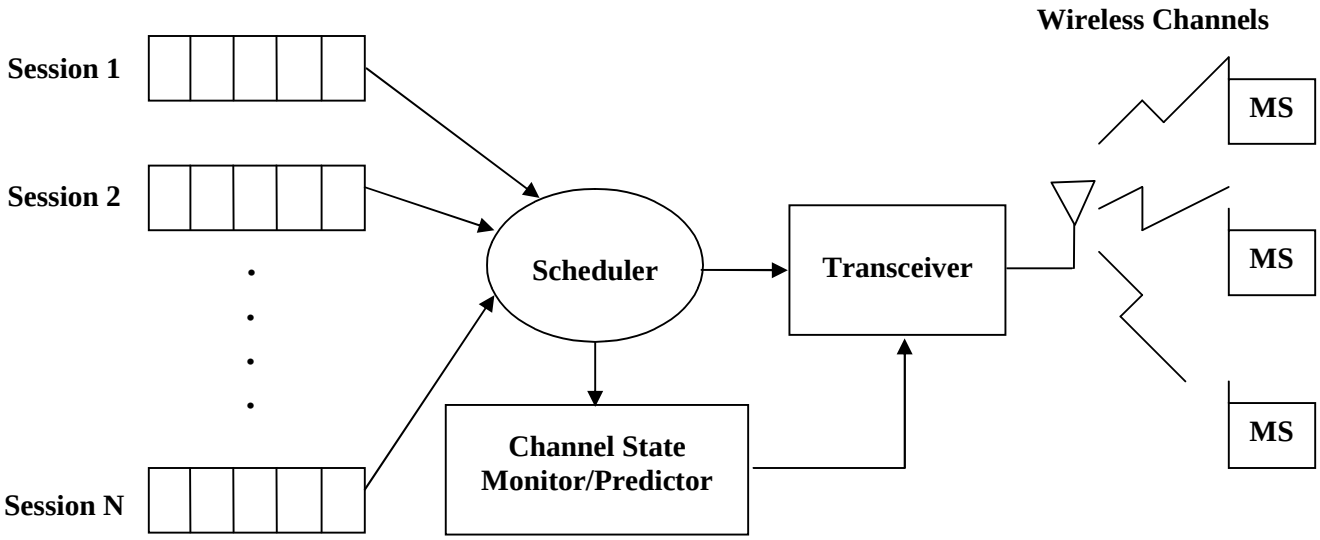

Figure 4-6 A Typical Wireless Scheduler, scheduling decisions are made for the forward linkk

4.2.2.1 Operation of the MAC Protocol

The operation of the implemented scheme can be divided into two phases. In the first phase the BS broadcasts request packets to all MS's, the request packet contains the mobile terminal id, type of service, BER estimate, exponential decay rms (ExpDecayTrms) and pilot symbols. The packet fields are described in more detail in the latter sections. On receiving the request packet, the MS sets the estimated BER as well as the other fields and retransmits the packet requesting for data service. The BS during the request phase collects all incoming transmission requests. The next phase is the information phase; here the BS makes scheduling decisions on the basis of available channel state information. The timeslot allocation algorithm can be conceptually represented as in Figure 4-7.

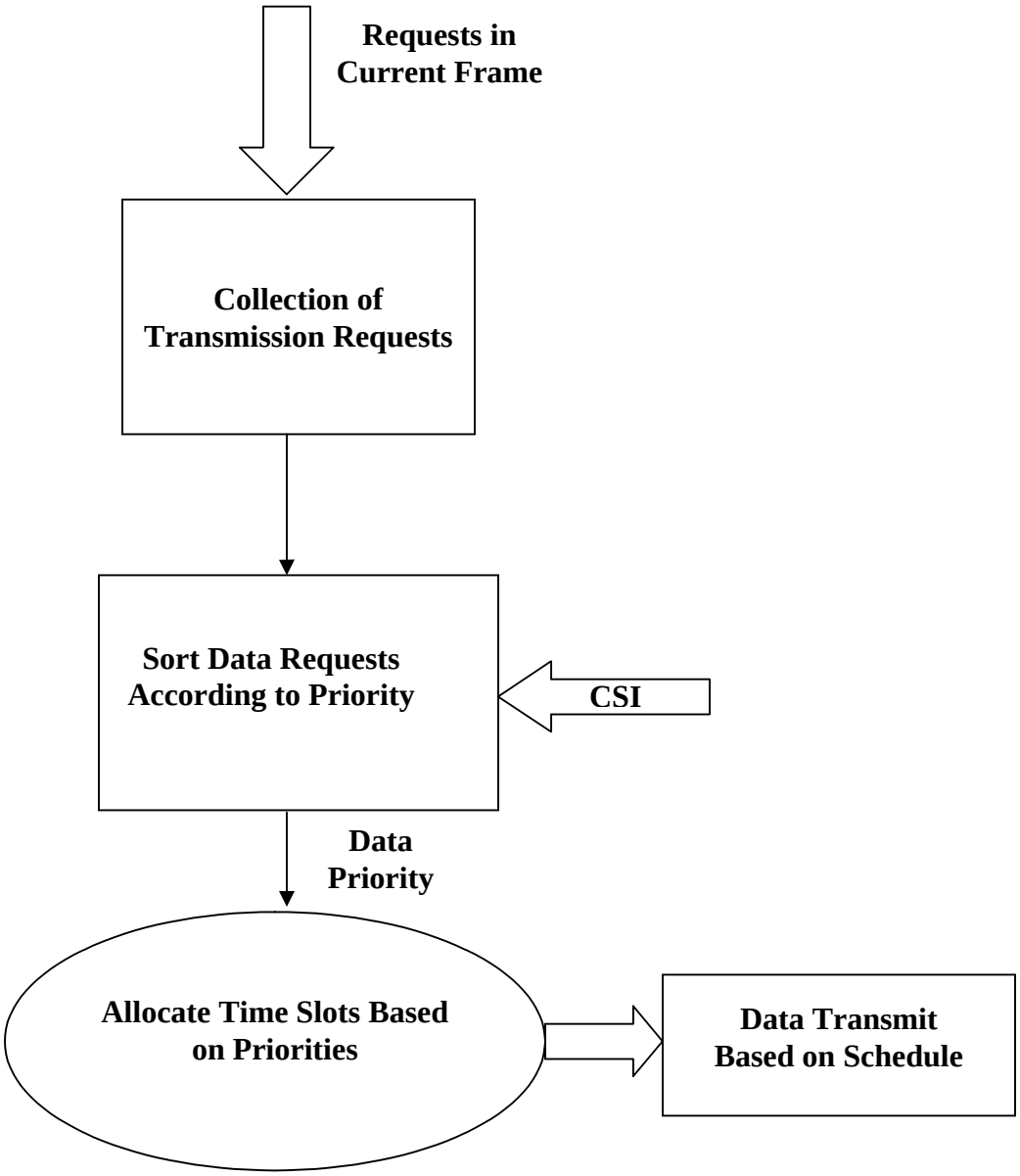

Figure 4-7 Time Slot Allocation Mechanism based on CSI from PHY Layer

The rationale behind such an algorithm is to give higher priority to mobile terminals that are in a better channel state during the bandwidth allocation process. The motivation comes from the fact that a user with a better channel condition with the support of the variable rate channel encoder can enjoy a higher transmission rate and can therefore utilize the system bandwidth more efficiently. Redundancy is incorporated into the information packet for error protection [36]-[38]. To exploit the time varying nature of

the wireless channel, a variable rate channel adaptive physical layer is employed. During the request phase all MS's send their CSI to the BS assuming the CSI remains approximately constant within a frame, it is thus appropriate to base the transmission mode for the whole frame (information packet transfer to the scheduled user) on the current CSI level. The adaptation thresholds are set such that a constant transmission target error level is observed. That is, when the channel condition is good, and it is possible to achieve a more than better error level, it would make more sense to switch to a higher transmission mode to better utilize the available bandwidth by still being able to maintain the target error level. On the other hand when the channel condition is bad, one can switch to a lower transmission mode. The block diagram of a variable rate channel encoder is shown in Figure 4-8.

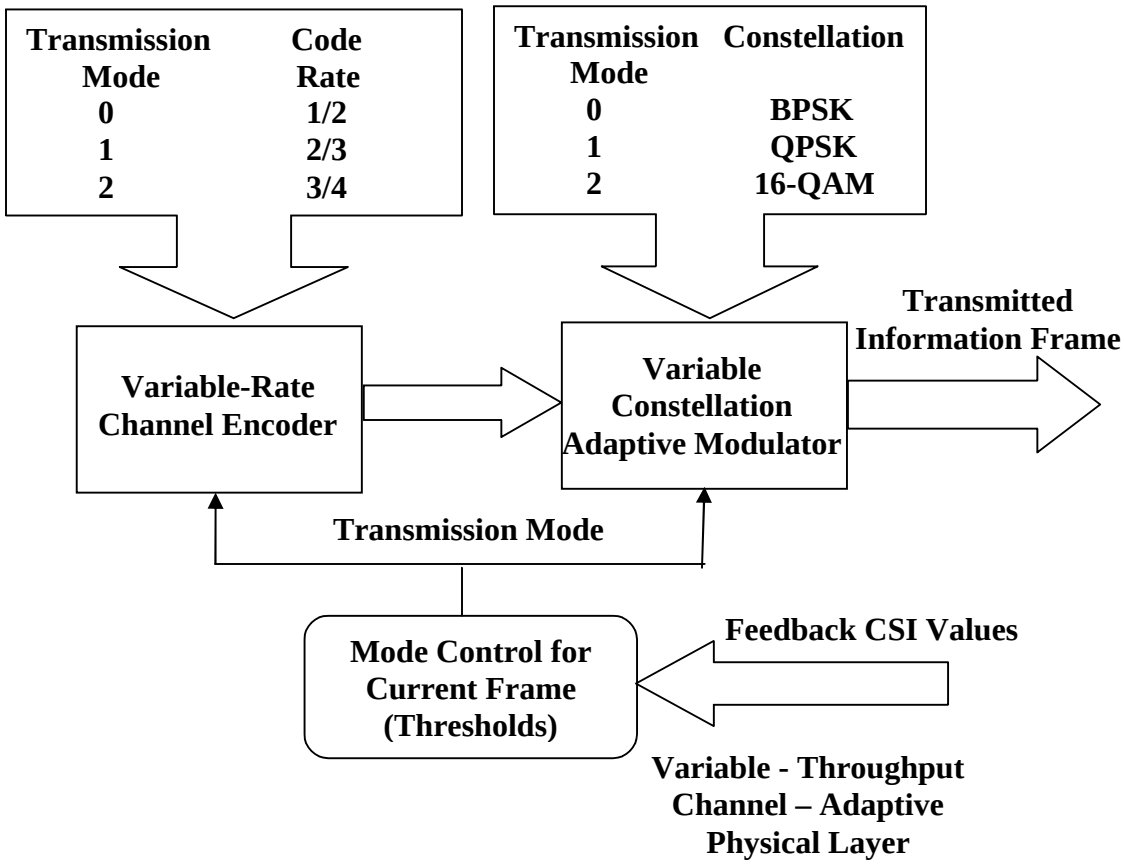

Figure 4-8 A Conceptual Block Diagram of the Variable-Rate Channel Adaptive Physical Layer

4.2.3 Network Layer Description

The system consists of a transmitter (BS) and arbitrary number of receivers (MS). Specifically, a cellular type of system is developed with information transfer taking place at the downlink. A number of uncoordinated users contend for the available bandwidth. In response to which, the BS implements a greedy scheduling algorithm that makes channel assignments based on the CSI. A detailed description on the DTDMA based MAC layer follows immediately after an introduction on scheduling strategies.

4.3 System Implementation

This section describes how the adaptive MAC system is implemented. This is followed by a sequence of sections detailing how each of the methodologies are implemented during this phase of research, with particular attention given to the description of how interfaces between layers (co-simulations) are established and the procedural steps used to implement the physical layer within the co-simulation.

4.3.1 System Overview

As shown in the palette of Figure 4-9, the system consists of two types of nodes: transmitters (BS) and receivers (MS). Each of these nodes may be fixed or mobile. In the following subsection we will give an elaborate description of each of these nodes.

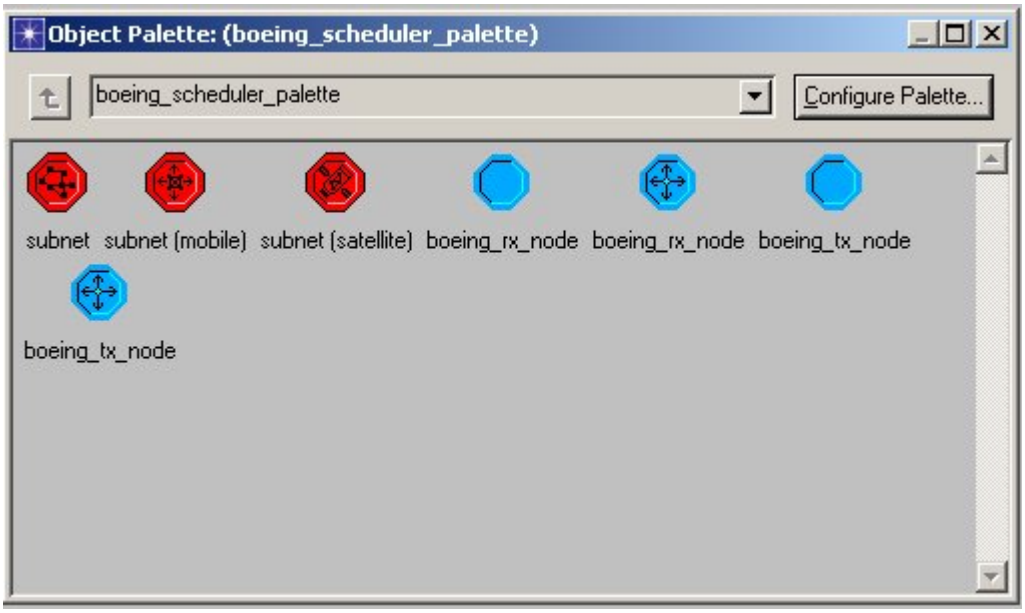

Figure 4-9 Object Palette with both transmitter and receiver nodes

4.3.2 Packet Editor

OPNET provides a packet editor to create custom packets suited for the application being considered. *Packet formats* define the internal structure of packets as a set of fields. For each field, the packet format specifies a unique name, a data type, a default value, a size in bits, an encoding style, a conversion method, and optional comments. Packet formats are referenced as attributes of transmitter and receiver modules within node models, in calls to Kernel Procedures (KP).

The system implementation requires two different packet types: control packets and the information packets. The *packet format* of a control packet is shown in Figure 4-10. The source generator at the transmitter module generates these control packets every 10 second interval. Next, the transmitter module (BS) broadcasts these control packets to all receivers (MS) that may in turn request data services in the downlink.

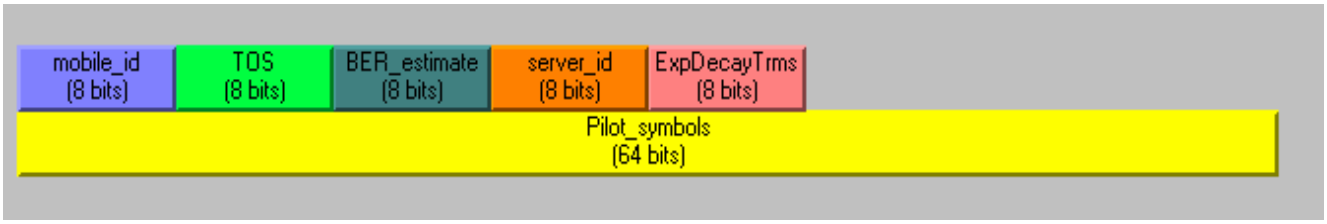

Figure 4-10 Packet format of control packets

The fields used are as follows:

- *mobile_id*: node id of the MS, this is set by the MS when it sends the control packet back to the BS after updating its channel state information. The packet is usually sent in the *request slot* when the MS wants to request a data service.
- *TOS*: type of service, specifies the type of service, either voice or data which the MS may request from the BS. Only data services are supported in the current implementation.
- *BER_estimate*: estimated BER value at the downlink, this field specifies the estimated BER value calculated using the physical layer simulator, from the B.S to the MS's. This forms the metric or the channel state information on the basis of which scheduling decisions are made.
- *server_id*: node id of the BS, this is typically a flag type that ensures that the *receiver section* of the BS does not receive the control packets when it is first broadcasted by the BS itself.
- *ExpDecayTrms*: rms value for calculating the exponential decay envelope that is required in the computation of a multipath channel impulse response. This field is required, since the channel is assumed to be almost constant over *k* frame durations. More specifically, since the channel conditions experienced by the downlink signal (either control of information packets) is different for each MS and because we estimate the channel only every *n*-sec interval we are required to make a supposition that the channel is almost constant till the next control packet is sent by the BS asking for channel state updates.
- *Pilot_symbols*: long training symbols are used for estimating the channel.

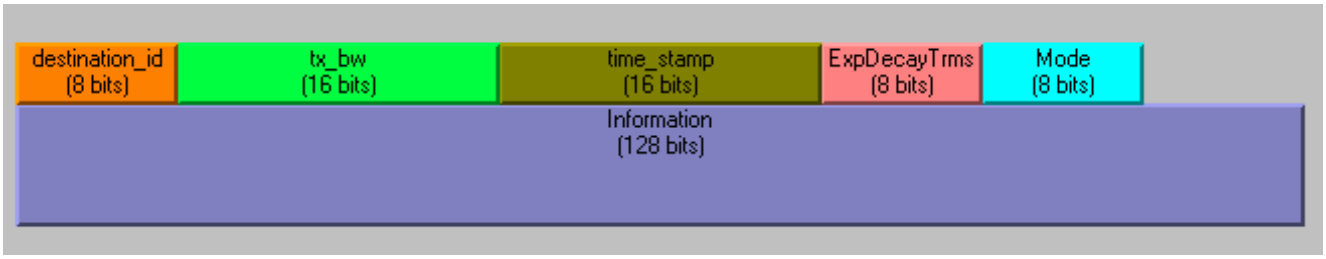

Figure 4-11 Packet format of information packets

After having received the control packets from the MS's that request a data service, the BS needs to make scheduling decisions based on the channel states of the contending users. Finally, having decided on which user to schedule, the *post_q/scheduler* transmits the information packets (see **Figure 4-11**) generated for that user, over the entire time slot. The fields used are as follows:

- *destination_id*: node id of the M.S to which the packet will be sent.
- *tx_bw*: transmission bandwidth to be allotted for a particular scheduled user. In our implementation, we allocate the entire bandwidth in a particular time slot, to the user with the best channel state.
- *time_stamp*: this is of particular importance for delay sensitive services such as voice, the time stamp holds the time instant at which the packet was created. It thus specifies the maximum amount of time the packet can be queued waiting for transmission, exceeding which it will be destroyed.
- *ExpDecayTrms*: rms value of the exponential decay envelope for generating a multipath channel impulse response, this field ensures that the channel condition is almost constant for the duration of information packet transfer from the time when the channel was first estimated to the time when channel estimate updates are requested again.
- *Mode*: this field specifies the transmission mode to be used in the downlink by the variable rate channel adaptive encoder. We have implemented a variable rate encoder that adaptively changes its modulation scheme and coding rate (transmission mode) depending on the channel conditions. Three different transmission modes are supported in our implementation.

- *Information*: information packets to be sent to the scheduled user.

4.3.3 Node Model of the BS

Figure 4-12 shows the node model of a BS that implements a greedy scheduling algorithm. The individual modules are as follows:

The *source_gen* module generates both control and information packets. Control packets are generated once every 10 seconds, whereas the information packets follow an exponential distribution with a mean interarrival rate of 1 second. Next, the control packets are sent directly to the *pkt_switch* module, whereas, the information packets are forwarded to a *pre_q* module.

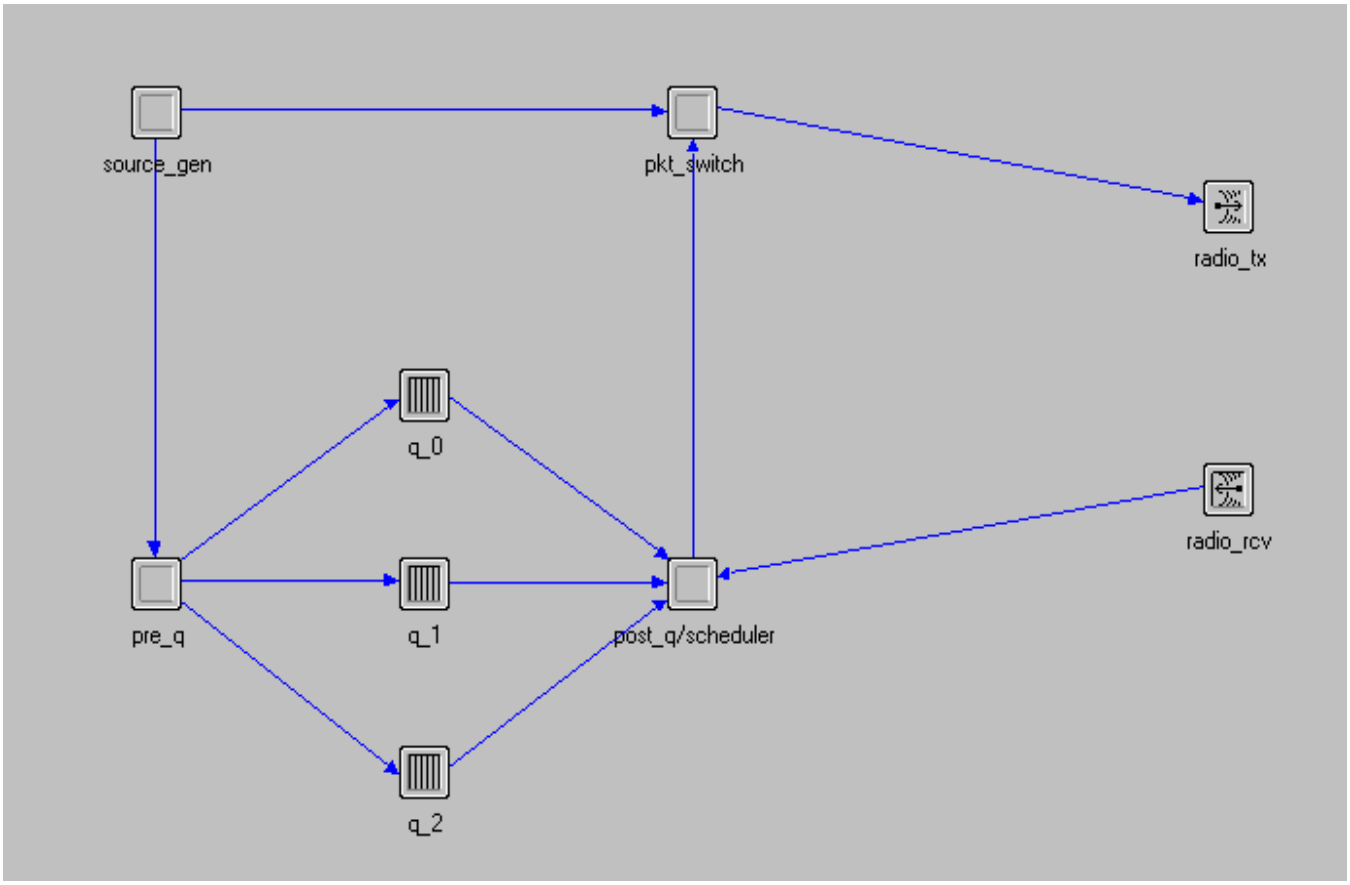

Figure 4-12 Node model of the transmitter (Base station)

The fields used are as follows:

- *pkt_switch*: this is basically a packet forwarder. The control packets received through its input stream is sent to the *radio_tx* wireless module that broadcasts the packet to all MS's. It also receives information packets from the *scheduler* for forwarding over the wireless channel through the *radio_tx* wireless section.
- *pre_q*: the function of this module is to set the destination i.d of the arriving information packets and then queue them in their respective buffers, waiting to be transmitted when a scheduling decision is made in their favor.
- *post_q/scheduler*: this is responsible for processing the control packets and making a decision as to which user to schedule depending on their channel states. Scheduling decisions are made once every 10 seconds, at this point the scheduler observes the stored table of BER estimates available at that time instant and makes a decision by scheduling the user with the lowest BER. Once, having decided which user to serve, the scheduler then forwards the packet generated for that user to the *pkt_switch* module, from here the packet is finally transmitted through the wireless transmit module.

4.3.4 Process Model Fundamentals

4.3.4.1 Source Generator

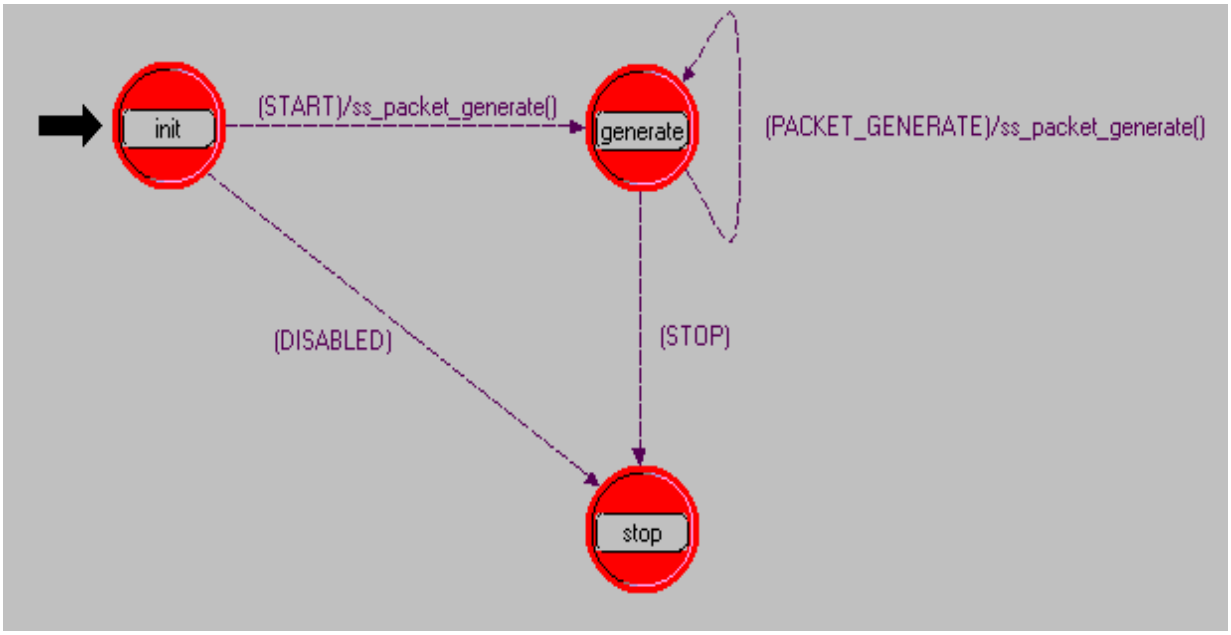

Figure 4-13 Process model of the source generator

Figure 4-13 shows the process model of the *source_gen* module of the BS. The FSM for this module consists of the following primary states:

init: initialization state, this state reads the values of source attributes and schedules a self interrupt that will indicate the start time for packet generation.

START/ss_packet_generate( ): this triggers an interrupt for packet generation. Two different types of packet formats are generated, these include the control packets that are generated once every 10 seconds and the information packets that are generated with a mean interarrival rate of 1 second (follows an exponential distribution). The packets are sent through different output streams into the subsequent stages.

generate: at the enter execs of the generate state, we schedule the arrival of the next packet. This is taken care of using the interarrival time specified by the user in the attributes section of the node model.

stop: when the control enters into the "stop" state, it is the time to stop generating traffic. The state cancels the generation of the next packet and goes into a silent mode by not scheduling anything else.

4.3.5 Scheduler

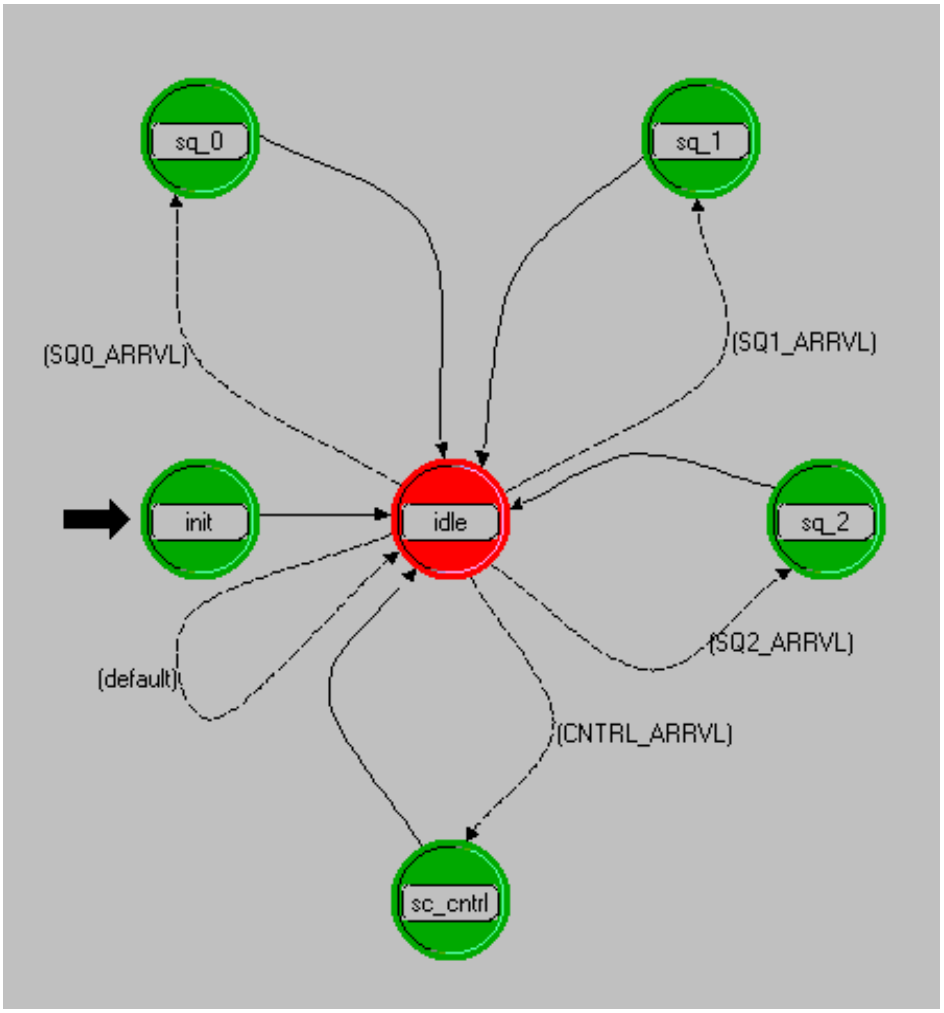

Figure 4-14 Process model of the post_q/scheduler section

Figure 4-14 depicts the process model of the *post_q/scheduler*. The FSM consists of the following primary states:

init: does flag initializations as well as attribute retrievals required by this module.

sc_cntrl: this corresponds to the scheduler portion of the process model. The estimated BER and exponential decay rms values of all incoming requests are stored in an array that is indexed using the mobile id of the request packet. At the scheduling instant, the BER estimate table is scanned for the lowest value of BER (the best channel state) and the corresponding mobile node is scheduled for the entire slot duration.

sq_0 – sq_2: when a particular mobile node has been scheduled based on its CSI, a flag equal to the mobile id of the scheduled user is set. This causes a transition to the corresponding *sq_mobile_id* state. Once inside this state, packets are retrieved from the respective queues and subsequently forwarded to the *pkt_switch* module for routing.

4.3.6 Packet Switch

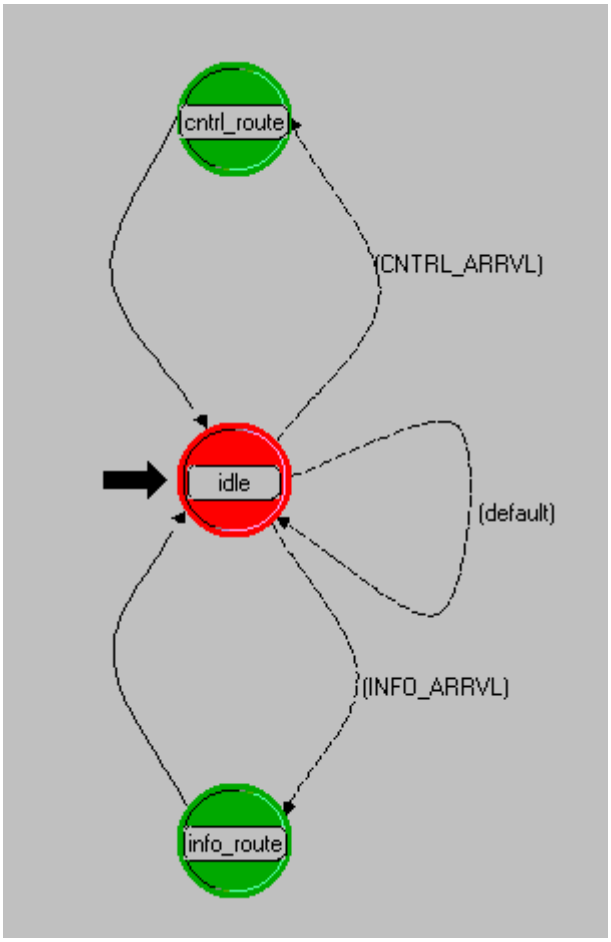

Figure 4-15 Process model of the *pkt_switch* module

Figure 4-15 depicts the process model of the *pkt_switch* section. This is basically a packet forwarder for both control and information packets. It consists of the following two primary states.

cntrl_route: An arriving packet from the *source_gen* module triggers an interrupt which results in the control being passed from the simulation kernel to the *cntrl_route* state. This in turn forwards the packet to the wireless transmit module for packet transmission.

info_route: An arriving packet from the *post_q/scheduler* module triggers an interrupt which results in the control being passed from the simulation kernel to the *info_route*

state. This in turn forwards the packet to the wireless transmit module for packet transmission.

4.3.7 Node Model of the MS

Figure 4-16 shows the node model of the M.S (receiver). It typically consists of the wireless radio transmit and receive sections, a receive processor module and a sink.

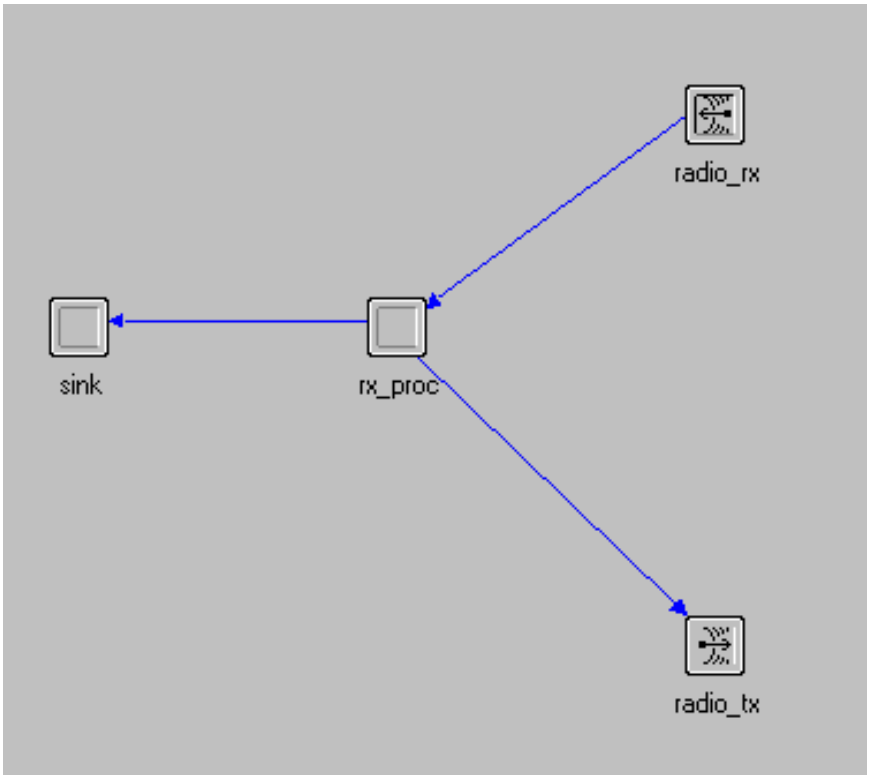

Figure 4-16 Node model of the receiver (mobile stations)

Here the *rx_proc* is responsible for processing incoming control packets and retransmitting them after updating its CSI. If the arriving packet is an information packet it is forwarded to the *sink*, which in turn records statistics and finally destroys the packet. For a more detailed description let us look at the process model of the *rx_proc* section.

Figure 4-17 depicts the process model of the *rx_proc* module. A packet arriving from the *radio_rx* wireless module triggers an interrupt to pass control the *rcv* state. The *rcv* state first checks if the arriving packet is a control or information packet. If the incoming packet is a control packet the state updates its CSI and retransmits it back to the B.S requesting for data service. If the arriving packet is an information packet, it is forwarded to the sink module that records statistics and finally destroys the packet.

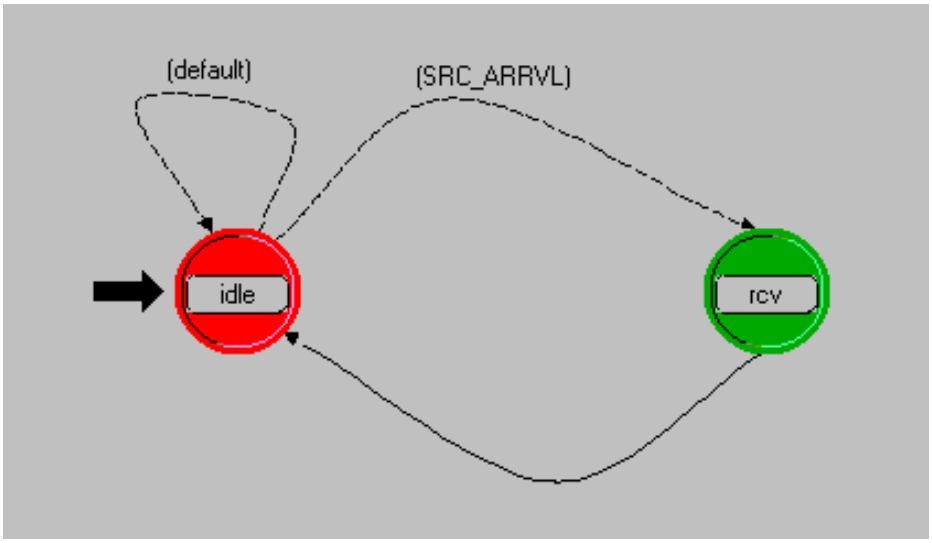

Figure 4-17 Process model of the *rx_proc* module

4.4 Simulation Description

4.4.1 Baseline System

4.4.1.1 Interface

The interface between OPNET and MATLAB is implemented using MATLAB engine routines. As part of the initialization routine of the Baseline System - I pipeline, the MATLAB engine is initialized and stored in an Engine variable. This variable is then

passed to the MATLAB *dra_ber* pipeline function. This allows OPNET to maintain multiple simultaneous MATLAB engines which may be useful when distinct variable namespaces are required.

4.4.1.2 Operations Performed in OPNET

The following are the tasks performed in OPNET:

- Identifying if the arriving packet is a control or information packet.
- If control packet, retrieve the modulation scheme and coding rate from the attributes table for each node (typically, BPSK and R½ convolutional code).
- If control packet, generate a random number between 1 and 5, each represents an exponential decay rms (simulates different channel conditions for each M.S).
- If information packet, extract the ExpDecayTrms field from the arriving packet (simulates the same channel condition as and when it was first simulated for the control packet). This ensures that the channel is almost constant for the entire time slot during which information packet transfer takes place.
- Initializing MATLAB engine.
- For control packets, call MATLAB function *runsim* with the inputs, Modulation, Coding Rate and ExpDecayTrms as estimated in steps 2 and 3 respectively.
- For information packets, call MATLAB function *runsim* with the inputs, Modulation, Coding Rate and ExpDecayTrms as estimated in steps 2 and 5 respectively (Fixed rate channel encoder uses BPSK and R½ convolutional code).
- Assign the average BER returned by the MATLAB routine to OPNET's packet transmission data OPC_TDA_RA_BER.

4.4.1.3 Operations Performed in MATLAB

The following are the tasks performed in MATLAB:

- Generating transmitted signal with specified Modulation and Coding Rate followed by the IDFT operation for OFDM signal generation.

- Generating different channel conditions for each M.S depending on its exponential decay rms field.
- Producing channel estimates based on the pilot symbols.
- Determine the average BER at a fixed average SNR of 10dB and using the other parameters specified by OPNET.

4.4.1.4 Procedural Description

A detailed procedural description of the Baseline System is omitted here for reasons of brevity as this would be explained in greater detail in the subsequent section that addresses the Full PHY-MAC layer system implementation. The two fundamental differences between the Baseline System and Full PHY-MAC layer system is that the Baseline System does not employ a variable rate encoder, also the MAC layer does not make scheduling decisions based on channel state information. Note that the Baseline System – I basically implements a round robin scheduling technique. At the request phase all incoming request are collected, meanwhile updating the ExpDecayTrms field for each mobile node. Following this the users are scheduled in a round robin manner. This ensures that all M.S get an equal share of the available channel bandwidth, but is characterized by the inherent limitation of reduced overall system throughput compared to Full PHY-MAC layer system. The results comparing both models will be elaborated in the last section of this report.

4.4.2 Full PHY-MAC Layer Implementation System

4.4.2.1 Interface

The interface between OPNET and MATLAB is implemented using MATLAB engine routines. As part of the initialization routine of the Full PHY-MAC layer pipeline, the MATLAB engine is initialized and stored in an Engine variable. This variable is then passed to the MATLAB *dra_ber* pipeline function.

4.4.2.2 Operations Performed in OPNET

The following are the tasks performed in OPNET:

- Identifying if the arriving packet is a control or information packet.
- If control packet, retrieve the modulation scheme and coding rate from the attributes table for each node (typically, BPSK and R½ convolutional code).
- If control packet, generate a random number between 1 and 5, each represents an exponential decay rms (simulates different channel conditions for each M.S).
- If information packet, extract the Mode (specifies modulation and coding rate) field from the arriving packet.
- If information packet, extract the ExpDecayTrms field from the arriving packet (simulates the same channel condition as and when it was first simulated for the control packet). This ensures that the channel is almost constant for the entire time slot during which information packet transfer takes place.
- Initializing MATLAB engine.
- For control packets, call MATLAB function *runsim* with the inputs, Modulation, Coding Rate and ExpDecayTrms as estimated in steps 2 and 3.
- For information packets, call MATLAB function *runsim* with the inputs, Modulation, Coding Rate and ExpDecayTrms as estimated in steps 4 and 5.
- Assign the average BER returned by the MATLAB routine to OPNET's packet transmission data OPC_TDA_RA_BER.

4.4.2.3 Operations Performed in MATLAB

The following are the tasks performed in MATLAB:

- Generating transmitted signal with specified Modulation and Coding Rate followed by the IDFT operation for OFDM signal generation.
- Generating different channel conditions for each M.S depending on its exponential decay rms field.
- Producing channel estimates based on the pilot symbols.

- Determine the average BER at a fixed average SNR of 10dB and using the other parameters specified by OPNET.

4.4.2.4 Procedural Description

Figure 18 shows the modified process flow for the *dra_ber* pipeline stage for the MATLAB implementation. Note that the purple boxes correspond to operations performed using OPNET KP's, black boxes correspond to operations performed using C routines, and blue boxes correspond to operations performed in MATLAB. Notice that C is only used to initialize parameters, to start the MATLAB engine, and to serve as an interface between OPNET and MATLAB. The use of the C routine to interface with MATLAB encapsulates the details of calling and using the MATLAB routines. To limit the possibility of memory leaks, all mxArrays created as part of the MATLAB interface are destroyed upon completion of that routine. Where possible, the vector processing capabilities of MATLAB are exploited within these functions in an effort to improve the execution speed of this code.

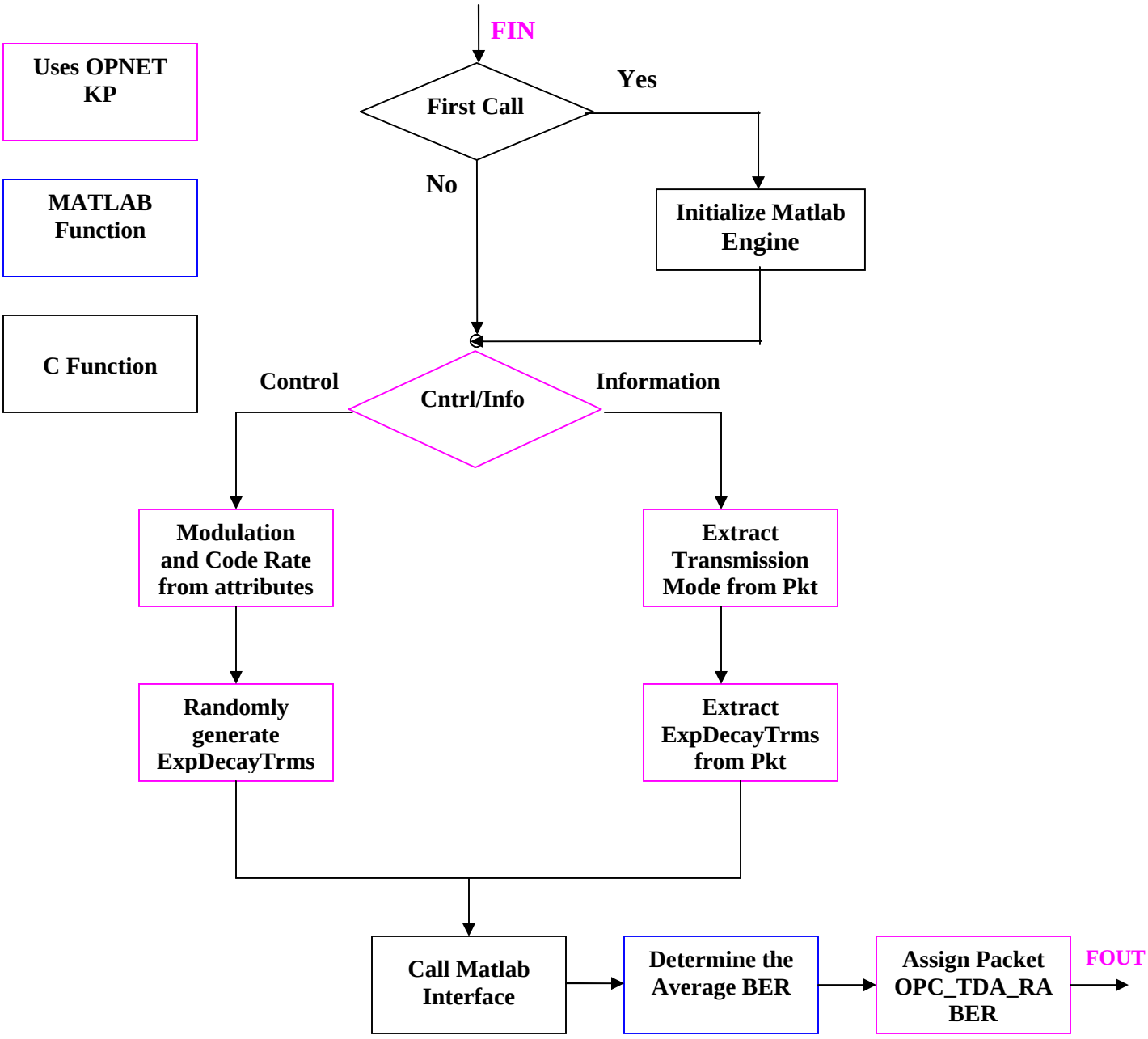

Figure 4-18 Modified process flow for *dra_ber* pipeline stage for physical layer simulation using OPNET

4.5 Results

This section describes the specific parameters used in the simulation and presents the results of the simulations performed using each of the different methodologies.

4.5.1 Scenario Description

The system consists of a fixed transmitter (BS) and three receiver nodes (MS's). Captured results are presented for both Baseline System as well as the full PHY-MAC layer system implementation. A number of additional scenarios can also be studied using the developed framework that would answer issues on scalability and other factors, these scenario descriptions and results are omitted here for brevity. A modified system that would support a large number of mobile nodes can be simulated by using a single queue process model for the BS and then stamping the information packet with the mobile id of the scheduled user just before data transmission.

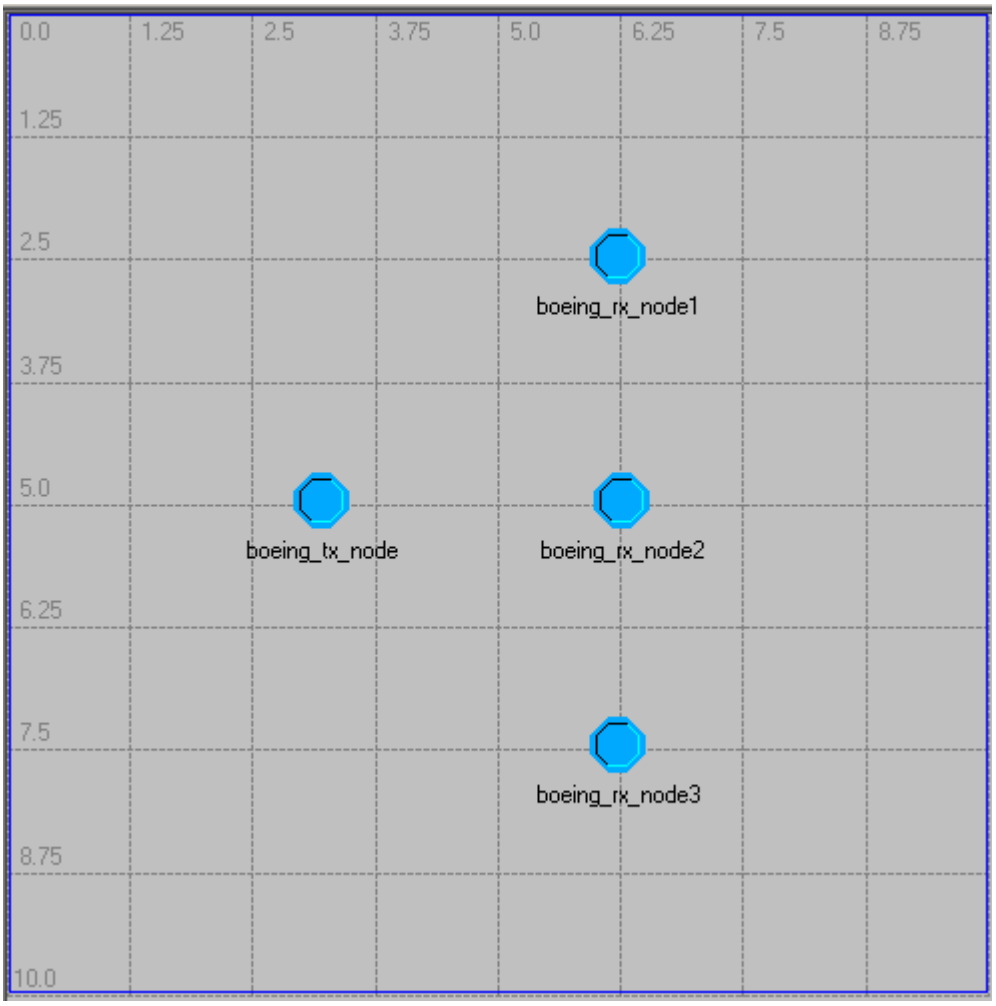

Figure 4-19 Network Scenario with one Tx Node and three Rx Nodes

4.5.2 Captured Results

This section lists the results captured for each of the simulation methods explored as part of this simulation. Specifically, end-to-end delay (ETE), and throughput (in bits) presuming packet rejection when any errors occur in the packet were measured, for each method considered in this scenario.

4.5.2.1 Baseline System

Figure 4-20 depicts the radio receiver throughput for each of the mobile stations when the B.S employs a round robin scheduling algorithm. This method implements a bandwidth allocation strategy that is channel independent. The main advantage with implementing this kind of a scheduling strategy is the fairness among sessions observed when doing long time scheduling operations. As seen in **Figure 4-20** the throughputs are almost equal for all three mobile stations because they are scheduled for equal time intervals.

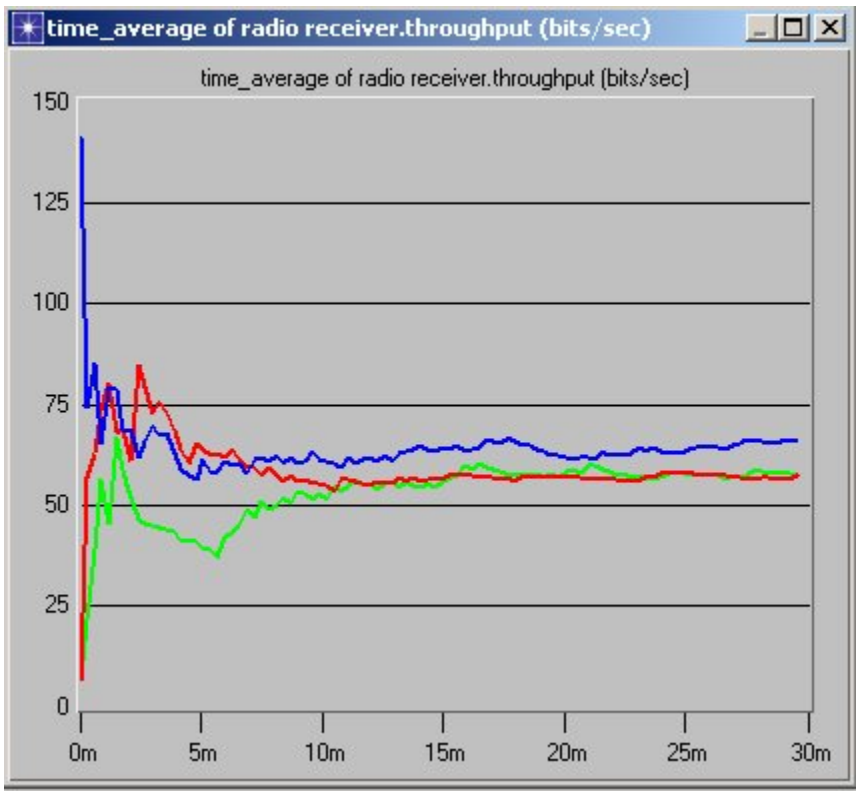

Figure 4-20 Radio receiver throughput comparison of different mobile stations

Next the end-to-end delay and global throughput of the system are studied. The scheduling strategy as seen from **Figure 4-21** is successful in maintaining a constant

throughput over long scheduling time duration. This very well satisfies the necessary performance criterion for most wireless schedulers, there is however, a relative shortcoming, this will be addressed in the subsequent subsection.

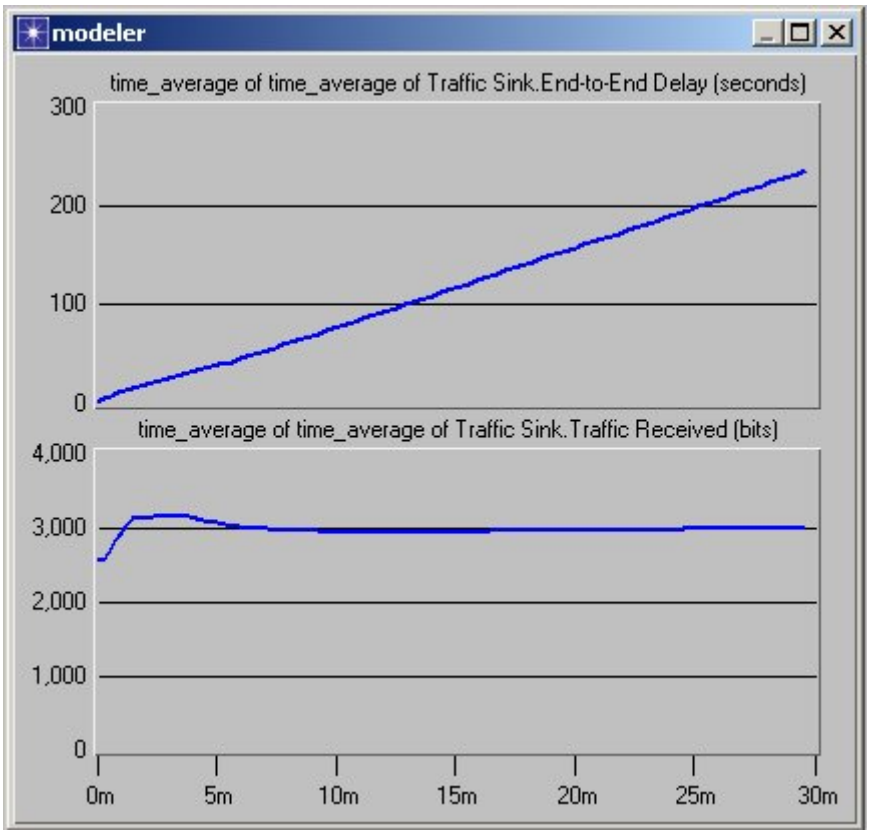

Figure 4-21 End-to-End Delay and Throughput Statistics for Baseline System

4.5.2.2 Full PHY-MAC layer simulation

Figure 4-22 shows the radio receiver throughput curves for the different mobile stations that contend for the available transmission bandwidth. Observe that mobile node 1 has a relatively higher throughput compared to nodes 2 & 3. This is because the full PHY-MAC layer system implements a greedy scheduling algorithm. It so happens that the channel state corresponding to the first node has been sufficiently good for a longer time

duration compared to the other two nodes and hence mobile node 1 was at most times scheduled to receive information packets from the BS. It is obvious that this scheme does not ensure fairness among sessions, but this can be easily incorporated into the current framework by just adding a waiting time field in the calculation of the scheduler metric.

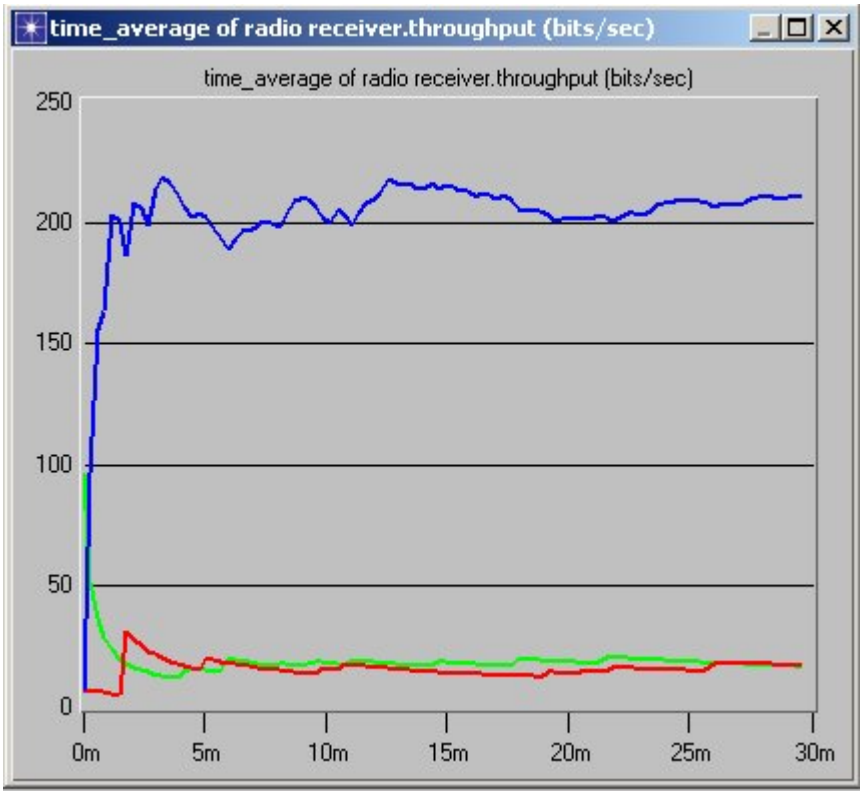

Figure 4-22 Radio receiver throughput comparison of different mobile stations

One of the more important conclusions can be drawn by making a comparison between Figures 4-21 and 4-23. Observe that the throughput of the full PHY-MAC layer system is relatively high compared to the Baseline System. In other words a greedy channel state dependent scheduling algorithm with a variable rate encoder at the physical layer

outperforms a round robin scheduler. This, in particular, is more owing to the synergy resulting due to the combination of the variable rate encoder and the DTMDA based MAC layer rather than the actual scheduling strategy itself. The full PHY-MAC layer implementation changes to a higher transmission mode when the channel condition is too benign. In such a scenario a higher transmission throughput can be obtained as more number of bits per symbol is transmitted with a higher signal alphabet. The Baseline System on the other hand uses the same modulation scheme and coding rate throughout information packet transfer and its scheduling decision does not depend on channel state information estimated in the downlink.

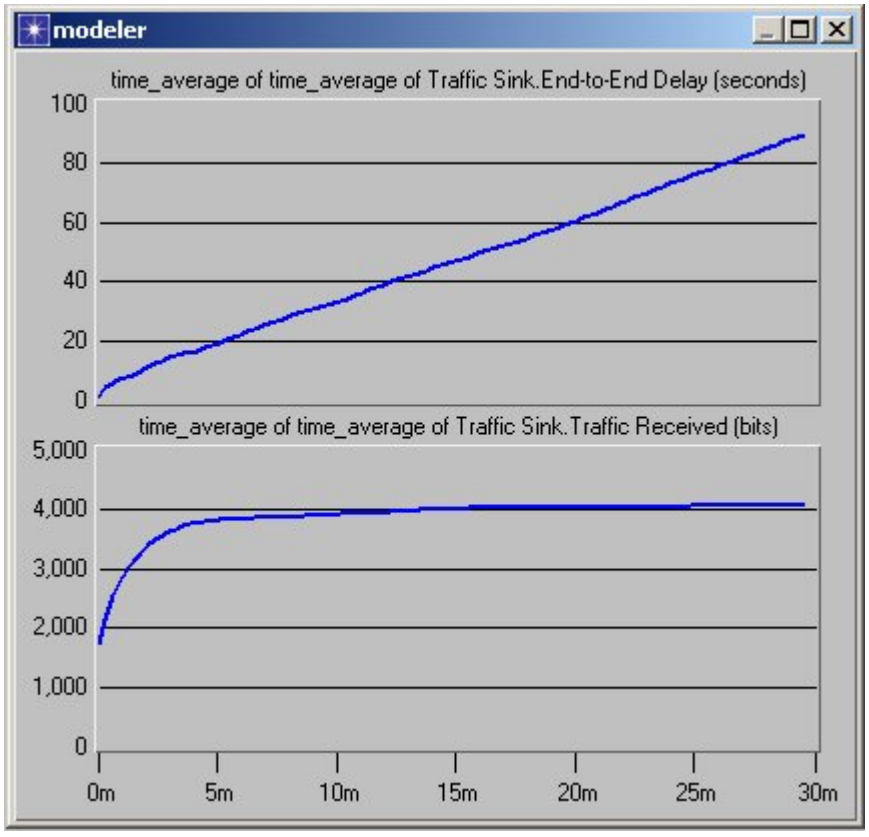

Figure 4-23 End-to-End Delay and Throughput Statistics for the Full PHY-MAC layer system

4.5.3 Simulation Benchmark

4.5.3.1 Fidelity Benchmark

Treating the full PHY-MAC layer simulation method as the benchmark, it can be seen from the results that the baseline method falls below in throughput statistics compared to the full PHY-MAC layer system.

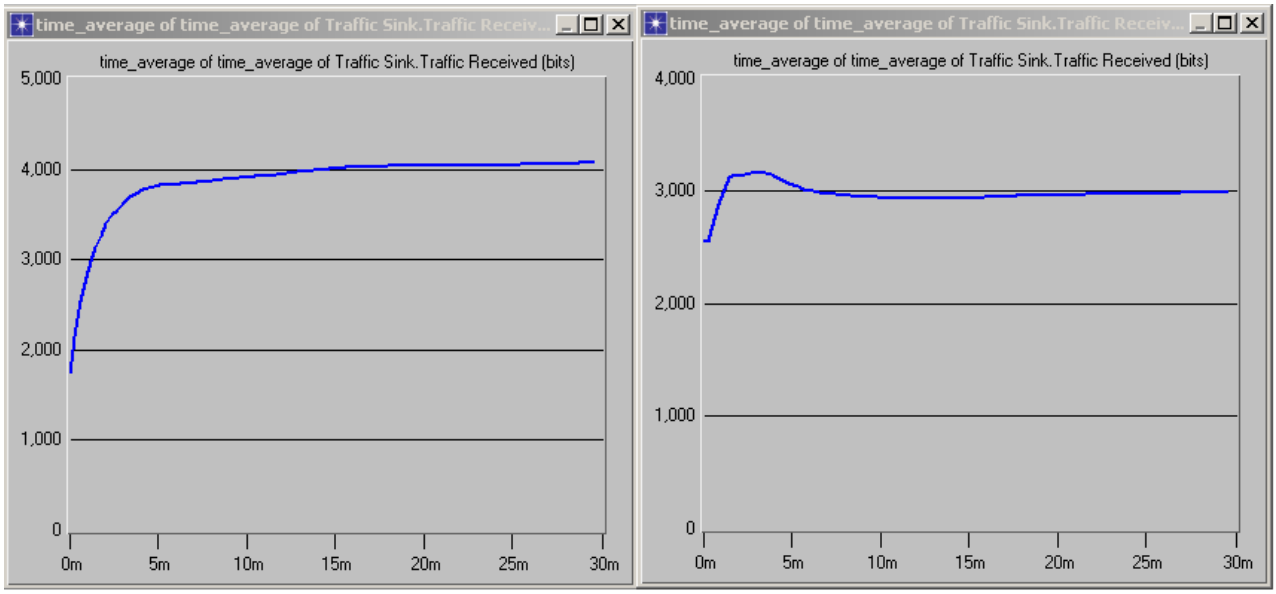

Figure 4-24 Comparison of throughput statistics between the Baseline system and the Full PHY-MAC layer system

Method	Fidelity
Baseline System	**Good**
Full PHY-MAC Layer System	**Perfect**

Table 4-2 Fidelity comparison between the Baseline and Full PHY-MAC layer system

4.5.3.2 Simulation Time Benchmark

Both the simulation approaches required processing from MATLAB and hence the simulation time in terms of events/second is relatively lower compared to traditional OPNET only simulation speeds, but the gains in terms of fidelity is promising. The simulation speeds can be considerably increased by writing the entire PHY layer simulator in C.

Method	Simulation Time (Events/sec)	Performance
Baseline System	**20**	**Good**
Full PHY-MAC Layer System	**18**	**Good**

Table 4-3 Performance comparison between the Baseline and Full PHY-MAC Layer system

4.6 Conclusion

The layering approach to the design of a protocol stack offers low complexity to communication system design but in order to improve overall system performance it is worthwhile to look into exploiting the synergy resulting from the combination of different protocol layers. This research investigated one such approach, in which a channel adaptive MAC protocol was used to gain higher overall system throughput. The proposed scheme employed a variable throughput adaptive channel encoder and modulator in the physical layer. Specifically, two types of systems were investigated as part of this work. The first was a Baseline system with a fixed rate channel encoder without any PHY and MAC layer interaction and the second was a Full PHY-MAC layer system that uses a variable rate channel encoder at the physical layer. Synergy was

achieved by the interaction between the PHY and MAC layer. The results clearly show the performance gains possible by employing such a scheme.

This simulation also demonstrated the need for cross-layer simulations for MANET and the viability of co-simulation of the physical layer. It should be noted that the novel cross-layer approach developed in this research opens the door as an excellent starting point for additional research in this area.

Chapter 5

Contributions and Future Work

5.1 Thesis Contributions

This thesis had two broad sets of concerns. In the first, the focus was on Multiple Antenna techniques, more specifically dealing with Selective Cochannel Interference Cancellation and Diversity Combining. And in the second, the main emphasis was on Adaptive MAC scheduling for Wireless Systems.

One of the most noteworthy contributions of this thesis was the development of an analytical framework for characterizing the outage probability and average error rates for i.n.d Rayleigh faded CCI signals. All previous literature on this subject chose an unrealistic i.i.d assumption for the cochannel interferers. Since the CCI signals are of dissimilar signal strengths in practical operating environments, the premise of i.n.d fading statistics for the cochannel interferers is more realistic. In addition the closed form outage probability expressions derived in this chapter are sufficiently general since they treat all common fading models for the desired user signal amplitude.

Next, the thesis investigated a hybrid AIN/MRC receiver. The analytical framework developed in this chapter answers to a great extent an open question pertaining to the selection of commonly employed schemes for reducing the detrimental effects of cochannel interference, AIN and MRC. Given constraints over the number of antenna elements, for a given operating SIR, there are instances where the hybrid AIN/MRC scheme may outperform a conventional AIN alone or MRC alone receiver. The derivation of a generic closed form expression for the outage probability and average error rates for the hybrid AIN/MRC receiver presented in this chapter also helps in evaluating the performance of the AIN alone or MRC alone receiver as a limiting case.

Finally, the concluding chapter looked into Adaptive MAC scheduling for wireless systems. This work exploits the benefits resulting from a synergy of the combination of the MAC and PHY layer of a wireless network through a cross-layer simulation perspective. Traditional simulation methodologies independently model the physical and network layer. When multiple layer simulations are required, an abstraction of one layer is inserted into the other in order to provide the multiple layer simulation. However, recent advances in wireless communication technologies, such as adaptive modulation and adaptive antenna algorithms, demand a cross-layer perspective to this problem in order to achieve a sufficient level of fidelity. This part of the research thus explored a very novel link layer control scheme with the inclusion of physical layer techniques in OPNET and has the paved the way to a plethora of interesting investigations that can be carried out in this area.

5.2 Suggestions for Future Work

This section enumerates some suggestions for future work that can be extended through work done as part of this thesis. With regards to the chapter dealing with the performance evaluation of mobile radio systems employing a SIC receiver, the pdf of the SIR is available in closed form only for the case of Rayleigh faded CCI signals with unequal signal strengths. This work can be extended for the case where the CCI signals follow any arbitrary fading distribution. Computationally possible error probability expressions though not in closed form can still be derived for these cases.

The research work on Adaptive MAC scheduling and in general cross-layer simulation methodologies provides an excellent starting point for additional research. For instance the MAC scheme can be fully implemented to further study the impact of Smart Antennas in a more realistic MANET scenario. Network layer issues could be studied such as the impact of physical layer and MAC layer algorithms on routing protocols in a MANET. Further work can also be done on implementation issues of layer specific processes.

References

[1] H. Fattah and C. Leung, "An efficient scheduling algorithm for packet cellular networks," *IEEE VTC-2002 Fall*, vol. 4, pp. 2419-2423.

[2] H. Fattah and C. Leung, "An overview of scheduling algorithms in wireless multimedia networks," *IEEE Wireless Communications Magazine*, pp. 76-83, Oct 2002.

[3] Y. K. N. Lau and Y. –K. Kwong, "On the synergy between adaptive physical layer and multiple-access control for integrated voice and data services in a cellular wireless network," *IEEE Transactions on Vehicular Technology*, vol. 51, pp. 1338-1351, Nov 2002.

[4] J. H. Winters, "Smart antennas for wireless systems," *IEEE Personal Communication Magazine*, pp. 23-27, Feb 1998.

[5] J. Hicks, S. Bayram, W. H. Tranter, R. J. Boyle and J. H. Reed, "Overloaded array processing with spatially reduced search joint detection," *IEEE Journal on Selected Areas in Communications*, vol. 19, pp. 1584-1593, Aug 2001.

[6] J. Tsai, J. Hicks and B. D. Woerner, "Joint MMSE beamforming with SIC for an overloaded array system," *Proc. '01 IEEE Conference on Military Communications*, vol. 2, pp. 1261-1265, 2001.

[7] M. S. Alouini, A. Bastami and E. Ebbini, "Outage probability of cellular mobile radio systems with successive interference cancellation," *Proc. '99 Asilomar Conference on Signals, Systems and Computers*, pp. 192-196, 1999.

[8] M. O. Hasna, M. S. Alouini, A. Bastami and E. S. Ebbini, "Performance analysis of cellular mobile systems with successive co-channel interference cancellation," *IEEE Transactions on Wireless Communications*, vol. 2, pp. 29-40, Jan 2003.

[9] A. Annamalai and V. Srivastava, "Outage probability of cellular mobile radio systems employing a selective co-channel interference cancellation scheme," *Proc. IEEE VTC 2001*, pp. 492-496. Also appeared in the *Wireless Communication and Mobile Computing Journal*, vol. 2, pp. 421-438, June 2002.

[10] R. Vaughan and W. Venables, "Permanent expressions for order statistic densities," *J. Royal Statistical Society*, vol. 34, no. 2, pp. 308-310, 1972.

[11] A. Annamalai, C. Tellambura and V. K. Bhargava, "Simple and accurate methods for outage analysis in cellular mobile radio systems – A unified approach," *IEEE Transactions on Communication,* vol. 49, no. 2, Feb 2001.

[12] Y. D. Yao and A. Sheikh, "Investigation into co-channel interference in microcellular mobile radio systems," *IEEE Transactions on Vehicular Technology*, vol. 11, pp. 114-123, May 1992.

[13] J. P. Linnartz, Narrowband land-mobile radio networks, MA: Artech, 1993.

[14] M. Abramowitz and I. A. Stegun, Handbook of mathematical functions with formulas, graphs and mathematical tables, NY: Dover publications, ninth ed., 1970.

[15] G. L. Stuber, Principles of mobile communications, Kluwer academic publisher, Boston: 1996.

[16] R. Prasad, Universal wireless personal communications, Artech House, Boston: 1998.

[17] A. Abu-Dayya and N. C. Beaulieu, "Outage probabilities of diversity cellular systems with cochannel interference in Nakagami fading," *IEEE Transaction on Vehicular Technology*, vol. 41, pp. 343-355, Nov 1992.

[18] V. A. Aalo and J. Zhang, "On the effect of cochannel interference on average error rates in Nakagami-fading channels," *IEEE Communication Letters*, vol. 3, pp. 136-138, May 1999.

[19] R. Mostafa, A. Annamalai and J. H. Reed "Performance evaluation of cellular mobile radio systems with adaptive interference nulling of dominant interferers," Submitted for publication.

[20] M. Hasna and M. S. Alouini, "Performance evaluation of cellular mobile systems with successive co-channel interference cancellation," *Proceedings of VTC 2000*, pp. 1506-1513.

[21] C. Tellambura and A. Annamalai, "An unified numerical approach for computing the outage probability for mobile radio systems," *IEEE Communication Letters*, vol. 3, pp. 97-99, April '99

[22] J. Abate and W. Whitt, "Numerical inversion of laplace transforms for probability distribution," *ORSA J. Computing*'95.

[23] J. Terry and J. Heiskala, *OFDM wireless LAN's: A theoretical and practical guide*, Sams Publishing 2002.

[24] R. V. Nee and R. Prasad, *OFDM for wireless multimedia communications*, Artech House Publishers, 2000.

[25] IEEE 802.11a, "Wireless LAN medium access control (MAC) and physical layer (PHY) specifications: High-speed physical layer in the 5GHz band," IEEE Std 802.11a-1999.

[26] HiperLAN/2, "Broadband radio access networks (BRAN); HIPERLAN Type 2; Physical layer," ETSI YS 101 475 V1.2.1 (2000-11).

[27] J. Hagenauer, "Rate compatible punctured convolutional codes and their applications," *IEEE Transactions on Communications*, vol. COM-36, pp. 389-400, April 1998.

[28] M. –H. Hsieh and C. –H. Wei, "A low complexity frame synchronization and frequency offset compensation scheme for OFDM systems over fading channels," IEEE Transactions on Vehicular Technology, vol. 48, Sept 1999.

[29] A. J. Goldsmith and S. Chua, "Adaptive coded modulation for fading channels," *IEEE Transactions on Communications*, vol. 45, pp. 1218-1230, May 1998.

[30] J. G. Proakis, *Digital Communications Fourth Edition*, New York, McGraw Hill, 2000.

[31] H. Zhang, "Service disciplines for guaranteed performance service in packet-switching networks," *Proc. IEEE*, vol. 83, pp. 1374-1396, Oct 1995.

[32] X. Liu, E. K. P. Chong, N. B. Shroff, "Opportunistic transmission scheduling with resource sharing constraints in wireless networks," *IEEE Journal on Selected Areas in Communications*, vol. 19, pp. 2053-2064, Oct 2001.

[33] S. Lu, V. Bharghavan and R. Sirkant, "Fair scheduling in wireless packet networks," *IEEE/ACM Transactions on Networking*, vol. 7, pp. 473-489, Aug 1999.

[34] T. Nandagopal, S. Lu and V. Bharagavan, "A unified architecture for the design and evaluation of wireless fair queuing algorithms," *ACM MOBICOM*, pp. 132-142, Aug 1999.

[35] R. Guerin and V. Peris, "Quality-of-service in packet networks: basic mechanisms and directions," *Computer Networking*, vol. 31, pp. 169-189, 1999.

[36] Y. K. N. Lau and Y. –K. Kwong, "Synergy between adaptive channel coding and media access control for wireless ATM," *in Proc. VTC '99Fall*, Sept 1999.

[37] V. K. N. Lau and S. V. Maric, “Variable rate adaptive modulation for DS-CDMA,” *IEEE Transactions on Communications*, vol. 47, pp. 577-589, Apr 1999.

[38] M. Kwagishi, S. Sampei and N. Morinaga, “A novel reservation TDMA based multiple access scheme using adaptive modulation for multimedia wireless communication system,” *in Proc. VTC’98*, pp. 112-116, 1998.